Replication Stress is an Actionable Genetic Vulnerability in Desmoplastic Small Round Cell Tumors

Asuka Kawai-Kawachi, Madison M Lenormand, Clémence Astier, Noé Herbel, Meritxell B Cutrona, Carine Ngo, Marlène Garrido, Thomas Eychenne, Nicolas Dorvault, Laetitia Bordelet, et al.

Replication stress is an actionable genetic vulnerability in desmoplastic small round cell tumors

Asuka Kawai-Kawachi[1,2,†], Madison M. Lenormand[1,3,†], Clémence Astier[1,4,†], Noé Herbel[1,4,5,6,7], Meritxell B. Cutrona[8], Carine Ngo[1,6], Marlène Garrido[1], Thomas Eychenne[1], Nicolas Dorvault[1], Laetitia Bordelet[9], Feifei Song[10], Ryme Bouyakoub[8], Anastasia Loktev[11], Antonio Romo-Morales[11], Clémence Hénon[1,5,6], Léo Colmet-Daage[1], Julien Vibert[1,5,6], Marjorie Drac[12], Rachel Brough[10], Etienne Schwob[12], Oliviano Martella[8], Guillaume Pinna[13], Janet Shipley[11], Sibylle Mittnacht[14], Astrid Zimmermann[15], Aditi Gulati[10], Olivier Mir[6], Axel Le Cesne[6], Matthieu Faron[6], Charles Honoré[6], Christopher J. Lord[10], Roman M. Chabanon[1,4,*] & Sophie Postel-Vinay[1,4,5,6,14, *]

[1]The ATIP-Avenir Inserm and ERC StG (Epi)genetic Vulnerabilities in Solid Tumors and Sarcoma Laboratory, Inserm Unit UMR 981, Université Paris-Saclay, Gustave Roussy, Villejuif, France
[2]Cancer RNA Research Unit, National Cancer Center Research Institute, Tokyo, Japan
[3]Department of Genomes and Genetics, Institut Pasteur, CNRS UMR3525, Paris, France
[4]Université Paris-Saclay, Université Paris-Sud XI, Faculté de Médicine, Le Kremlin Bicêtre, France
[5]Drug Development Department, DITEP, Gustave Roussy, Villejuif, France
[6]Sarcoma Committee, Gustave Roussy, Villejuif, France
[7]Viroxis SAS Biotech, Gustave Roussy, Villejuif, France
[8]Organoid Core Facility, Gustave Roussy, Villejuif, France
[9]Experimental and Translational Pathology (PETRA) Platform, AMMICa Unit (CNRS Unit UMS 3655, Inserm Unit US 23), Gustave Roussy, Villejuif, France
[10]The CRUK Gene Function Laboratory and Breast Cancer Now Toby Robins Research Centre, The Institute of Cancer Research, London, United Kingdom

[11]Sarcoma Molecular Pathology Team, Divisions of Molecular Pathology and Cancer Therapeutics, The Institute of Cancer Research, London, United Kingdom
[12]Institute of Molecular Genetics, CNRS Unit UMR 5535, Université de Montpellier
[13]RNA Interference Platform PARi, IRCM/IBFJ/CEA UMRE008, Fontenay-aux-Roses, France
[14]UCL Cancer Institute, University College London, London, United Kingdom
[15]Research Unit Oncology, the Healthcare Business of Merck KGaA, Darmstadt, Germany

Running title. Targeting replication stress in DSRCT.

Keywords. PARP inhibitors, ATR inhibitors, EWS-WT1, replication stress, DSRCT, cGAS/STING.

† **Joint first authorship**

*** Co-corresponding authors**:

Mail	Email	Phone
114 rue Edouard Vaillant 94800 Villejuif, France	sophie.postel-vinay@gustaveroussy.fr	+33(0)142114211
114 rue Edouard Vaillant 94800 Villejuif, France	roman.chabanon@gustaveroussy.fr	+33(0)142114211

Conflict of Interest and Financial Disclosure. NH declares employment and research funding by Viroxis SAS biotech. AZ declares employment by Merck KGaA. OM is an employee and shareholder of Amgen, Inc. SPV has received research funding from Hoffman La Roche and AstraZeneca for unrelated research projects. As part of the Drug Development Department (DITEP), SPV is principal investigator or sub-investigator of clinical trials from Abbvie, Agios Pharmaceuticals, Amgen, Argen-X Bvba, Arno Therapeutics, Astex Pharmaceuticals, Astra Zeneca, Aveo, Bayer Healthcare Ag, Bbb Technologies Bv, Blueprint Medicines, Boehringer Ingelheim, Bristol Myers Squibb, Celgene Corporation, Chugai Pharmaceutical Co., Clovis Oncology, Daiichi Sankyo,

Debiopharm S.A., Eisai, Eli Lilly, Exelixis, Forma, Gamamabs, Genentech, Inc., GlaxoSmithKline, H3 Biomedicine, Inc, Hoffmann La Roche Ag, Innate Pharma, Iris Servier, Janssen Cilag, Kyowa Kirin Pharm. Dev., Inc., Loxo Oncology, Lytix Biopharma As, Medimmune, Menarini Ricerche, Merck Sharp & Dohme Chibret, Merrimack Pharmaceuticals, Merus, Millennium Pharmaceuticals, Nanobiotix, Nektar Therapeutics, Novartis Pharma, Octimet Oncology Nv, Oncoethix, Onyx Therapeutics, Orion Pharma, Oryzon Genomics, Pfizer, Pharma Mar, Pierre Fabre, Roche, Sanofi Aventis, Taiho Pharma, Tesaro Inc, and Xencor. SPV has participated to advisory boards for Merck KGaA. CJL makes the following disclosures: receives and/or has received research funding from: AstraZeneca, Merck KGaA, Artios, Neophore. Received consultancy, SAB membership or honoraria payments from: Syncona, Sun Pharma, Gerson Lehrman Group, Merck KGaA, Vertex, AstraZeneca, Tango, 3rd Rock, Ono Pharma, Artios, Abingworth, Tesselate, Dark Blue Therapeutics, Pontifax, Astex, Neophore, Glaxo Smith Kline. Has stock in: Tango, Ovibio, Hysplex, Tesselate. CJL is also a named inventor on patents describing the use of DNA repair inhibitors and stands to gain from their development and use as part of the ICR “Rewards to Inventors” scheme and also reports benefits from this scheme associated with patents for PARP inhibitors paid into CJL’s personal account and research accounts at the Institute of Cancer Research. All other authors have no conflicts of interest or financial interests to disclose.

Word count / Metrics

Abstract: 223 / 250

Manuscript text: 7389 / 7500

6 Figures

17 Supplementary Figures

Abstract (233 / 250 words)

Desmoplastic small round cell tumor (DSRCT) is an aggressive sarcoma subtype of high unmet need that is driven by the EWS-WT1 chimeric transcription factor. To identify novel therapeutic approaches to the targeting of DSRCT, we conducted a high-throughput drug sensitivity screening assessing chemosensitivity profiles for 79 small-molecule inhibitors on the JN-DSRCT-1 cell line. We found DSRCT cells to be sensitive to PARP and ATR inhibitors (PARPi, ATRi), as a monotherapy and in combination. These effects were recapitulated using multiple clinical PARPi and ATRi in three biologically distinct, clinically-relevant models of DSRCT, including cell lines, a patient-derived xenograft (PDX)-derived organoid, and a cell line-derived xenograft mouse model. Mechanistically, exposure to a combination of PARPi and ATRi caused increased DNA damage, G2/M checkpoint activation, micronuclei, replication stress, and R-loop formation. EWS-WT1 silencing abrogated these phenotypes and was epistatic with exogenous expression of the R-loop resolution enzyme RNase H1 in reversing the sensitivity to PARPi and ATRi monotherapies, suggesting that EWS-WT1-dependent increase in R-loop formation could be a mechanistic cause of drug sensitivity in DSRCT cells. Combination of PARPi and ATRi further induced an EWS-WT1-dependent cell-autonomous activation of the cyclic GMP-AMP synthase/stimulator of interferon genes (cGAS/STING) innate immune pathway and cell surface expression of programmed-death ligand-1 (PD-L1). Taken together, our findings point towards a role for EWS-WT1 in generating R-loop-dependent replication stress and provide a rationale for the clinical assessment of PARPi and ATRi in DSRCT.

Statement of significance: 29 / 32 Words

We show that EWS-WT1, the unique oncogenic driver of DSRCT, confers sensitivity to PARP and ATR inhibitors, thus providing a rationale for assessing these drugs in patients with DSRCT.

Introduction

Desmoplastic small round cell tumor (DSRCT) is a rare and aggressive subtype of sarcoma, affecting predominantly young males (1). DSRCT classically presents as a large abdominal mass and is most often diagnosed at advanced or metastatic stages with multiple peritoneal metastatic nodules, and sometimes distant metastases. Clinical prognosis for advanced DSRCT remains poor with a 5-year survival rate below 15% (2). No major therapeutic advance has occurred for DSRCT over the past 20 years, and currently, DSRCT patients undergo a standard Ewing sarcoma regimen, consisting of highly aggressive poly-chemotherapy and extensive surgical debulking (1). Therefore, the development of novel therapeutic strategies is urgently needed.

DSRCT is molecularly characterized by the t(11;22)(q13;q12) chromosomal translocation, which fuses the transactivation domain of *EWSR1* to the DNA binding domain of *WT1,* encoding an aberrant chimeric transcription factor (2,3). The presence of *EWSR1::WT1* rearrangement is pathognomonic of the disease and provides the diagnosis of DSRCT over other small round cell sarcomas (2). Recent genomic sequencing identified rare additional secondary mutations, notably in genes encoding proteins involved in chromatin remodeling and DNA repair such as *ARID1A*, *KMT2C*, and *MSH3* (4–7). EWS-WT1 conditional expression in mesenchymal stem cells – the putative cell-of-origin of DSRCT – is necessary and sufficient to generate a DSRCT phenotype (8), and EWS-WT1 is considered as the unique driver in this simple-genomics sarcoma (9). As such, this chimeric aberrant transcription factor represents the most evident

therapeutic target in DSRCT. However, the direct targeting of transcription factors is extremely challenging (10), and one of the most promising strategies, which consists of degrading the target transcription factor, is just entering the clinic and has not yet been evaluated in transcription factors-driven sarcomas. Therefore, targeting downstream consequences of EWS-WT1 presence, such as transcription factor-induced oncogenic programs or replication stress, is an attractive strategy.

In this study, we aimed to identify novel actionable targeted dependencies in DSRCT, using functional genomics and small-molecule inhibitor screening. We found that two distinct DSRCT cell lines, one newly-established patient-derived xenograft (PDX)-derived organoid (PDX-O) model and one cell line-derived xenograft mouse model were selectively sensitive to poly-ADP-ribose polymerases inhibitors (PARPi) and ataxia-telangectasia and Rad3-related inhibitors (ATRi). Mechanistically, we found that the presence of EWS-WT1 increased DNA replication stress and R-loop formation, thereby causing enhanced reliance upon the ATR/CHK1 pathway. Exposure to PARPi and ATRi further activated the cyclic GMP-AMP synthase/stimulator of interferon genes (cGAS/STING) pathway and caused PD-L1 upregulation in DSRCT cell lines, suggesting potential for these drugs as DNA repair-targeted therapies and immunomodulators in DSRCT.

Materials and Methods

Cell lines

The DSRCT JN-DSRCT-1 (JN1) cell line was purchased from American Type Culture Collection (ATCC). The DSRCT R cell line was created in-house, derived from a patient-derived xenograft (PDX) shared by Dr. Armelle Logié-Dishington (Champions Oncology, France). Briefly, the PDX was finely minced into tiny pieces that were subsequently washed in fetal bovine serum (FBS) and centrifuged. The pellet was resuspended in DMEM/F12 supplemented with 20% FBS, 1X MEM non-essential amino acids (#11140050, Gibco) and 1X Pen-Strep (#15070063, Gibco), and incubated in a 10 cm² petri dish at 37°C and 5% CO_2. The culture medium was changed every other day with recovery of suspended cells by centrifugation at 1200rpm. After 6-8 weeks, a partially homogeneous cell layer was obtained; from this primary culture, cells were washed with 1X phosphate buffered saline (PBS), dissociated in trypsin-EDTA solution (#25200056, Gibco), and seeded into a new culture flask for subsequent cell culture. JN1 and R cells were cultured in DMEM/F12, supplemented with 10% or 20% of FBS, respectively. A673 and SaOS-2 cells were cultured in DMEM, supplemented with 10% FBS. All cells were grown at 37°C and 5% CO_2. Mycoplasma testing was performed bimonthly using the MycoAlert Mycoplasma Detection Kit (Lonza). All cell lines were short-tandem-repeat typed using StemElite ID (Promega) to confirm identity.

The JN1 and R cell lines were originally derived from human tumors that were histopathologically diagnosed as DSRCT (11): the JN1 cell line was established

from a 7-year old male metastatic DSRCT patient's pleural effusion and harbors the following pathognomonic *EWSR1::WT1* fusion 3'-[CCCATGGATGAAGGACCAGATCTTGATCTAG]-[GTGAGAAACCATACCAGTGTGACTTCAAGG]-5' (**Supp Fig. S1**); the R cell line was established from a 20-year old male metastatic DSRCT patient's lymph node and harbors the following pathognomonic *EWSR1::WT1* fusion 3'-[GGAGAGCGAGGTGGCTTCAATAAGCCTGGTG]-[GTGAGAAACCATACCAGTGTGACTTCAAGG]-5' (**Supp Fig. S2**). The Ewing sarcoma A673 cell line was gifted by Dr. Olivier Delattre (Institut Curie, France) and the osteosarcoma SaOS-2 cell line was gifted by Dr. Olivia Fromigue (Gustave Roussy, France).

Generation of RNase H1-overexpressing JN1 cells

To generate stable RNase H1-expressing JN1 (JN1-RNaseH1 cell line), the ppyCAG-RNaseH1-V5 plasmid (Addgene, #111906) was transfected in JN1 cells with Lipofectamine 2000 (Thermo Fisher) according to manufacturer's instructions. Stable pools of transfectants were generated by selection with hygromycin B and the resultant selected populations were submitted to clonal isolation using the limiting dilution method. Clones were recovered and profiled for RNase H1 expression by western blot.

Drugs and chemicals

The PARP inhibitors olaparib (AZD2281), talazoparib (BMN-673) and veliparib (ABT-888), the ATR inhibitors gartisertib (M4344), ceralasertib (AZD6738) and berzosertib (M6620), the CHK1 inhibitors prexasertib (LY2606368) and SRA-

737, as well as cisplatin, topotecan, and SN-38, were purchased from Selleck Chemicals. The ATR inhibitor tuvusertib (M1774) was provided by Merck (Darmstadt, Germany). Inhibitor stock solutions were prepared in dimethylsulfoxide (DMSO) and stored in aliquots at -80°C. Mitomycin C (MMC), thymidine, iodo-deoxyuridine (IdU), and 5-chloro-2′-deoxyuridine (CldU) were purchased from Sigma-Aldrich. PicoGreen® was purchased from ThermoFisher.

Small-molecule inhibitor and drug screen

The small-molecule inhibitor and drug screen was performed as described previously (12). Briefly, small molecules were purchased as solid from suppliers listed in **Supp Table S1** and stored in DMSO. Prior to the 384 well-plate screen, solid small molecules were resuspended in DMSO as 10 mM stocks, prior to further dilution in DMSO to create 384 well-plates containing a titration (0.5, 1, 5, 10, 50, 100, 500, 1000 nM). A Hamilton Microlab Star liquid handling platform was used for this and all subsequent liquid handling steps except for cell seeding.

JN1 cells growing in log phase were seeded in 384 well-plates at 250 cells per well in 50 µL of culture medium using a Thermo Fisher Multi-Drop Combi. This plating density was optimized to ensure that the cells were in growth phase by the end of the five-day treatment. 24 h after seeding, the medium was removed and replaced with medium containing the small molecule inhibitor library, as detailed above. Cells were then continuously cultured in the presence of small molecule inhibitors for a period of five days, at which point cell viability was estimated by adding 20 µL of CellTiter Glo® (Promega), diluted 1:4 in PBS to

the medium. After 10 min incubation at room temperature, the CellTiter Glo®-generated luminescence was captured using a Victor X-Light plate reader. Luminescence values from each well were normalized to the median of signals from wells exposed to DMSO only (in absence of small molecule inhibitor) to generate surviving fractions (SF). In total, the cell line was screened three times, generating triplicate SF data sets. Surviving fractions were then used to plot dose-response survival curves, generated using 3-parameter logistic regression analysis via the drc R-package20. Using drc, Area under the curve (AUC) values were calculated from dose-response survival curves. AUC values were expressed as the proportion of the maximum area, representing no response to a drug. They were further scaled to lie between 0 and 1. AUC values that were greater than 1 were capped to 1. Unscaled AUC values for each drug were also standardized, generating robust Z-scores based upon the median AUC effect in a panel of 92 cancer cell lines (**Supp Tables S2-S4**) and the median absolute deviation of these effects. Z-scores were then plotted as a waterfall plot.

2D cell-based assays

Cells were plated in 96-well plates at 7000 cells per well for JN1 cells and 10000 cells per well for R cells and continuously exposed to the drugs for a period of 7 days in culture. In the case of siRNA transfection, cells were transfected in 6-well plates 48 h prior to drug exposure and trypsinized and reseeded at the density specified above in 96-well plates 24 h prior to drug exposure. Cell viability was estimated by the addition of 50µL of CellTiter-Glo® Luminescent Cell Viability Assay (Promega), diluted in 1:4 in PBS. After 10 min

incubation at room temperature, the CellTiter Glo®-generated luminescence was captured using a Victor X-Light plate reader. Luminescence values from each well were normalized to the median signal of wells exposed to DMSO (vehicle) to generate surviving fractions (SF). Surviving fractions were then used to plot dose-response survival curves using GraphPad Prism.

For synergy analyses, cells were seeded in 96-well plates and continuously exposed to increasing concentrations of talazoparib (1:4 serial dilution, range: 0-500nM) and/or M4344 (1:3 serial dilution, range: 0-1000nM) for 7 days in culture. Cell viability was assessed as described above. The median response of replicates was normalized per median marginal value (i.e. response in absence of treatment). Synergy analysis was performed using R package synergyfinder. Dose-response curves for single drugs were fitted to a four-parameter log-logistic model. Synergy scores were calculated using the Bliss independence model.

3D spheroids assay

To form spheroids, 500 JN1 cells in 200 µL of media were plated into each well of 96-well ultra-low attachment plates (#7007, Corning). Once spheroids reached an area of ~200,000 μm^2, they were subjected to treatment with increasing concentrations of M6620 or SRA-737, in presence or absence of SN-38 (at 0.25 or 0.5 nM) for 5 days, with drug-containing media replenishment after 3 days. At day 5, the media was removed and replaced with fresh media, and spheroids size was monitored for up to 19 days after treatment start, using a Celigo™ imaging cytometer (Revvity).

Development of patient-derived xenografts (PDXs)

The establishment of PDXs was conducted as previously described (13). All animal procedures and studies were performed in accordance with the approved guidelines for animal experimentation by the ethics committee at University Paris Sud (CEEA 26, project 2014_055_2790) following EU regulation. Animals were housed under pathogen-free conditions with food and water ad libitum. At 1–12 h following the patient biopsy, fresh tumors fragments were implanted under the renal capsule of 6–8-wk-old male NOD scid gamma (NSG) mice obtained from Charles River Laboratories.

Derivation of DSRCT 3D organoid cultures from a PDX tumor biopsy

A PDX model was first established from the primary peritoneal tumor of an 11-year-old male patient with DSRCT. From this PDX, a tumor biopsy was taken and divided into various pieces for downstream processing, including the derivation of DSRCT 3D primary organoid cultures, referred to as GR_13 PDX-derived organoid (PDX-O). For cell dissociation, a sample of the biopsy (~100 mm3) was preserved in tissue storage solution (#130-100-008, Miltenyi Biotech) at 4ºC, and processed in less than 1 h. The sample was minced into small pieces that were subsequently digested in 5 mL of HBSS Hank's buffer with calcium and magnesium (#24020091, Gibco), containing 7.4 mg/mL collagenase type-II (#17101-015, Gibco) for 1 hour at 37ºC. The digestion was stopped by adding 20 mL of Advanced DMEM/F-12 (#12634028, Gibco) supplemented with 1X Pen-Strep (#15070063, Gibco) and 10% FBS

(#SV30160, Hyclone). The homogenate was passed through a 100-µm cell strainer (#542000, Greiner Bio-one) to remove debris and cell clumps, and the cell suspension was then centrifuged for 10 min at 450g. After aspiration of the supernatant, the cell pellet was re-suspended in 1 mL of the above-mentioned blocking medium.

To obtain DSRCT human tumor cells and separate them from mouse cells, we used a cell depletion kit (#130-104-694, Miltenyi Biotech). Briefly, the cell suspension was centrifuged for 10 min at 450g and re-suspended in 80 µL of PBS containing 0.5% w/v BSA. Mouse cells were magnetically labeled by incubating the cell suspension with 20 µL of mouse depletion cocktail for 15 min in the refrigerator. Human tumor cells were obtained from the flow-through, after passing the labelled cell suspension using magnetic separation and LS columns (#130-122-729, Miltenyi Biotec).

PDX-O culture

The cells were counted and plated in 96-well U-bottom ULA wells (#7007, Corning; or #650970, Greiner Bio-one) to ensure the formation of organoids in each well (5,000 viable cells in 100 µL of complete organoid medium per each well). The medium was refreshed every week by aspirating and adding 50 µL of complete organoid medium in each well, and the organoids were passaged every 3-4 weeks. The basal organoid medium formulation consisted of Advanced DMEM/F12 (#12634028) supplemented with 10 mM HEPES (#15630049), 1% GlutaMAX (#35050038), 1X B27 supplement (#17504044), 1% penicillin/streptomycin (#15140122), 1X N-2 (#17502048; all from Thermo

Fisher Scientific); 5% FBS (#F7524, Sigma Aldrich); 50 µg/mL Primocin (#Ant-pm-05, Invivogen) and 10 µg/mL Fungin (#Ant-fn-1, Invivogen). To obtain the complete organoid medium, the basal medium was supplemented with 1 mM N-acetylcysteine (#A72250, Sigma), 10 mM Nicotinamide (#N0636, Sigma), 10 ng/mL recombinant human RSPO-3 (#120-44, Preprotech), 10 ng/mL recombinant human Wnt3a (#HZ-1296, Proteintech), 10 ng/mL LIF (#HZ-1292, Proteintech), 25 ng/mL (#HZ-1325, Proteintech), 10 pg/mL IL6 (#HZ-1019, Proteintech), 50 ng/mL recombinant human FGF-basic (#100-18B, Preprotech) and 100 ng/mL recombinant human IGF (#100-11, Preprotech). 10 µM ROCK Inhibitor Y-27632 (#S1049, Selleckem) was added at the initial culture. The cells were plated using 8-channel VIAFLO electronic pipettes (#4624 and #4626, Integra). Finally, the plates were centrifuged for 5 min at 450g.

PDX-O drug combination survival assay

After 3 weeks of culture, 240 GR_13 organoids were manually collected from the 96-well plates, transferred into an Eppendorf tube and centrifuged for 5 min at 450g. The pelleted organoids were washed three times with 1X PBS and dissociated with TrypLE Express enzyme (#12604-013, Thermo Fisher Scientific). Next, the cells were filtered using a 70-µm cell strainer (#542070, Greiner Bio-one) and re-suspended in complete organoid medium. For the drug combination survival assay, 4,000 cells were seeded in 40 µL of complete organoid medium per well in U-bottom 96-well plates (#4515, Corning). The formation of organoids was monitored for 3 days through brightfield acquisition every 24h using an Incucyte® SX1 (Sartorius), prior to adding the drugs. Serial

five-fold dilutions of talazoparib or M4344 were prepared to yield final concentrations ranging from 50 µM to 16 nM (talazoparib) or 10 µM to 64 nM (M4344) in complete organoid medium. A 7x7 dose-response matrix was constructed, and each drug was also used alone to generate reference curves for each individual compound. DMSO at a concentration of 0.3% was included as a negative control (mock) for normalization purposes. Topotecan at a concentration of 1 µM was included as a positive control and to evaluate the quality of the assay. All treatments were prepared at 10X concentration, and 4.4 µL of each mixture were added to the initial 40 µL of organoid culture in the wells. Three technical replicates were used in each experiment. All plates were imaged through brightfield acquisition every 24h for 7 days using an Incucyte® SX1 (Sartorius) to monitor the PDX-Os response to treatments. To visualize the live/dead nucleated cells in PDX-Os, the dual-fluorescence Cyto3D Live-Dead assay (#BM01, Tebubio) was applied at 1% v/v in each well, following manufacturer's recommendations. Dual-fluorescence viability signal and brightfield images were acquired with Incucyte SX1 (Sartorius), and correlative measures of cell viability were subsequently obtained by use of CellTiter Glo® 3D (#G9682, Promega) on the same wells after 7 days, following manufacturer's instructions.

Immunofluorescence and image analysis

For the detection of γH2AX, RAD51 foci and micronuclei, cells were seeded in black 96-well plates (Greiner Bio-One #655090) at a density of 12,000 cells per well and exposed to the indicated drugs for 72 h. Cells were then fixed in 4%

paraformaldehyde for 20 min at RT, washed twice with PBS and permeabilized with 0.5% Triton X-100 in PBS for 10 min. Cells were then blocked in IFF (2% BSA, 2% FBS in PBS) for 1 h at RT and incubated with primary antibodies (RAD51, Abcam ab133534; γH2AX, Millipore 05-636; dilution 1:1000 in IFF) at 4°C overnight. Cells were then washed twice with PBS and incubated with Alexa Fluor 488-conjugated rabbit (ThermoFisher A-11008, dilution 1:1000) or Alexa Fluor 647-conjugated mouse secondary antibodies (Thermofisher A-21235, dilution 1:1000) and 1µg/mL DAPI. For micronuclei assessment, cells were incubated with PicoGreen® (1:400 with IFF). Cells were then washed twice with PBS, and 100µl PBS was added to each well prior to imaging. Plates were imaged using ImageXpress Micro Confocal High-Content Imaging System (Molecular Devices). Nine independent and randomly selected sites were scanned per well. Quantification of the number of γH2AX foci, RAD51 foci and micronuclei was performed under identical microscopy settings between samples, using the MetaExpress image analysis system (MolDev).

DNA fiber combing

JN1 cells were grown in 100mm dishes and synchronized using a double-thymidine block. Synchronized cells were transfected with EWS-WT1 or CCND1 siRNAs as described above. After 8 h, cells were continuously exposed to either DMSO control, talazoparib, M4344 or a combination of both for 6 h. For replication fork labeling, cells received pre-warmed medium containing 100µM CldU and were incubated at 37°C, 5% CO2 for 30 min. Cells were then rinsed 3 times with pre-chilled PBS and incubated with 100µM IdU for 30 min. Cells were

collected in cold PBS, counted and adjusted to 50,000 cells per 50µL PBS on ice. Plugs were generated by adding 50µL of pre-warmed 1% low-melting point agarose to the cells. The resulting 100µL mix was gently homogenized and quickly transferred into a casting mold and incubated for 1 h at 4°C to solidify. Subsequent steps were performed as previously described (14). For the analysis, initiation, termination and cluster patterns of replicative forks were considered to measure fork velocity.

Statistical analyses

Apart from the mouse xenograft experiment, no statistical methods were used to predetermine sample size and experiments were not randomized. The investigators were not blinded during xenograft experiments. Unless otherwise stated, all graphs show mean values with error bars (standard deviation, SD); 95% confidence intervals were used and significance was considered when * $P < 0.05$, ** $P < 0.01$, *** $P < 0.001$, **** $P < 0.0001$; ns, not significant.

Data availability

The raw data generated in this study are available upon request from the corresponding authors.

Additional methods details are available in Supplementary Information. All uncropped images of the blots included in this study are also available in Supplementary Information.

Results

Small-molecule inhibitor screening identifies PARP and ATR as targetable vulnerabilities in DSRCT

To identify candidate therapeutic targets for DSRCT, we conducted a high-throughput small molecule inhibitor-sensitivity screen in the JN-DSRCT-1 (JN1) cell line, using an in-house curated library of 79 anti-tumor agents and small-molecule inhibitors that are either in clinical use or in late-stage clinical development (12) (**Fig. 1A, B**; **Supp Table S1**). We calculated normalized Area Under the Curve (AUC) Z-scores from dose-response survival curves of each drug in the JN1 cell line (**Supp Table S3**) and compared them with those of a panel of 92 tumor cell lines previously screened with the same library (**Supp Table S4**) (12). This identified several DNA repair inhibitors as being highly toxic to the JN1 cell line, including three clinical PARP inhibitors (PARPi; talazoparib, olaparib and rucaparib, ranked #6, #7, and #9, with Z-scores of -2.018, -1.828 and -1.762, respectively), and one ATM/ATR inhibitor (ATRi; KU60019, ranked #18; Z-score -1.2225). Several conventional cytotoxic agents that are in clinical use for the treatment of DSRCT were also identified, such as etoposide and doxorubicin (ranked #4 and #18, respectively; **Fig. 1B**).

Because PARPi are already approved in solid tumors and are evaluated in combination with ATRi in multiple clinical trials, including in pediatric populations (15), these small molecule inhibitor classes harbored a high potential for immediate clinical translatability and we selected them for further validation. We conducted validation experiments using several clinical PARPi and ATRi in two

DSRCT cell lines: the JN1 cell line and a novel cell line, named “R”, which we created from a patient-derived xenograft (PDX, gift from Champions Oncology). The A673 (Ewing sarcoma) and SaOS-2 (osteosarcoma) cell lines were used comparatively as a sensitive and a resistant control sarcoma model, respectively, based on publicly available PARPi and ATRi sensitivity datasets (GDSC database and Holme et al. (12)). Dose-response survival assays confirmed the sensitivity of JN1 cells to two clinical-grade PARPi (talazoparib and olaparib) and two clinical-grade ATRi (AZD6738 and M4344), with SF50 values similar to that of the PARPi-sensitive A673 cell line (**Fig. 1C-F**; JN1 vs. A673: talazoparib, $p = 0.0095$; olaparib, $p < 0.0001$; AZD6738, $p < 0.0001$; M4344, $p < 0.0001$; two-way ANOVA). When comparing the SF50 of PARPi and ATRi found in the JN1 cell line with the corresponding average steady-state or max single-dose plasma concentrations ($C_{ss\text{-}mean}$ or $C_{sd\text{-}max}$, respectively) dosed in patients enrolled in pharmacokinetics studies and treated at the recommended phase 2 dose (16–18), we observed that the concentrations we used in vitro seemed clinically achievable (talazoparib, SF50 ≃ 10 nM, $C_{ss\text{-}mean}$ = 7 nM; olaparib, SF50 ≃ 1 µM, $C_{ss\text{-}mean}$ = 1.7 µM; AZD6738, SF50 ≃ 0.5 µM, $C_{sd\text{-}max}$ = 4.5 µM; M4344, SF50 ≃ 7 nM, $C_{sd\text{-}max}$ = 750 nM) – though no robust conclusion could be drawn at this stage considering the difficulties in comparing *in vitro* data to exposure in patients. We therefore further compared the sensitivity to talazoparib or olaparib of the JN1 cell line with that of other sarcoma cell lines in publicly available datasets (DepMap Broad Institute, **Fig. 1G, H**; Sarcoma CellMinerCDB (19), **Supp Fig. S3A, B**), and found that JN1 was at least as sensitive to the PARPi olaparib and talazoparib as Ewing

sarcoma cell lines, consistent with their previously reported sensitivity to PARPi(20).

R cells also showed sensitivity to ATRi but were resistant to PARPi, with an SF50 similar to that of the PARPi-resistant SaOS-2 cell line (**Fig. 1C-F**; R vs. SaOS-2: talazoparib, $p < 0.0001$; olaparib, ns; AZD6738, $p < 0.0001$; M4344, $p < 0.0004$; two-way ANOVA). This prompted us to explore the known causes of primary resistance to PARPi, such as the loss of PARP1 expression, which abrogates the PARP1 trapping-mediated cytotoxicity of PARPi (21). To test this hypothesis, we first evaluated PARP1 protein expression levels in JN1 and R cells by western blot and found that R cells displayed a significantly lower expression of PARP1 compared to JN1 cells (**Supp Fig. S4A**). To further establish a causative link between PARP1 expression and sensitivity to PARPi in DSRCT cells, we then evaluated the effects of silencing *PARP1* on the sensitivity of JN1 and R cells to PARPi. siRNA-mediated knockdown of *PARP1* conferred resistance to PARPi in JN1 but not R cells (**Supp Fig. S4B, C, E, F**). In addition, we noted that *PARP1* silencing did not affect the sensitivity of JN1 cells to veliparib – a PARPi with limited ability to trap PARP1 despite its ability to inhibit PARylation (22,23) (**Supp Fig. S4D, G**). Together, these findings suggest that PARP1 expression is a determinant of PARPi sensitivity in DSRCT cell lines, and that PARP1 trapping contributes to the cytotoxic effect of PARPi in DSRCT.

To next explore the applicability of our findings to patient's tumors, we analyzed:

(i) PARP1 expression by RNA-Seq (29 samples (24)); (ii) PARP1 expression by immunohistochemistry (IHC, 16 samples); and (iii) PARylation levels by IHC (i.e., levels of poly-ADP-ribose, the product of PARP1 activity; 16 samples) in two DSRCT cohorts. This revealed that PARP1 was highly expressed in a large majority of the cases (24 of 29 samples (82,8%) with PARP1 expression >10 TPM by RNA-Seq, and 14 of 16 samples (87,5%) with PARP1 H-score ≥200 by IHC; **Fig. 2A**; **Supp Fig. S5A**) and active (all samples with PARylation H-score ≥200 by IHC; **Fig. 2B**) as previously reported (20). Since PARPi are mostly toxic by trapping PARP1 onto the DNA, we therefore assumed that our conclusions may be applicable to most DSRCT. We further noted that the patients whose tumors harbored higher PARP1 transcript levels tended to have a longer overall survival, although this did not reach significance (**Supp Fig. S5B**).

Combination of PARP and ATR inhibitors shows synergistic effects in preclinical models that express PARP1

Because several PARPi plus ATRi combinations are currently being investigated in early-phase clinical trials (e.g. NCT04972110, NCT03462342), we evaluated this combination in DSRCT cell lines. Synergy scores calculated according to the Bliss independence method showed a synergistic interaction of the talazoparib and M4344 combination in JN1 (Bliss synergy score = 15.69; **Fig. 2C**, **Supp Fig. S6A**) but not R cells – where a modest additive effect could be observed, consistent with the limited sensitivity of the latter cell line to PARPi monotherapy (Bliss synergy score = 3.96; **Fig. 2D**, **Supp Fig. S6B**). Since

CHK1 inhibitors (CHK1i), which control the same cell cycle checkpoint and signaling pathway as ATRi, have also been evaluated in DSRCT in combination with irinotecan (NCT04095221), we further evaluated combination of PARPi with CHK1i. In our original screen, the evaluated CHK1i displayed limited cytotoxic effects in monotherapy in the JN1 cell line (SAR-20106, rank #39, Z-score = -0.697; PF-00477736, rank #55, Z-score = -0.197). We therefore used the clinical-grade CHK1i prexasertib and found additive effects with talazoparib in the JN1 cell line (Bliss synergy score = 6.00) but not R cell line, again consistent with the limited sensitivity of the latter to PARPi monotherapy (**Supp Fig. S6C-F**). Since PARPi and irinotecan – which is part of the chemotherapy regimen for patients who suffer from DSRCT – have some partly overlapping mechanism of action through DNA double-strand breaks formation, we assessed the combination of SN-38 (the active metabolite of irinotecan) with two clinical compounds that target the G2/M cell cycle checkpoint: the ATRi M6620 and the CHK1i SRA-737. Using a 3-dimensional (3D) spheroid model derived from the JN1 cell line that represents DSRCT cell physiology better than 2D cultures, we found that both inhibitors enhanced the cytotoxic effects of irinotecan – with M6620 showing potentially the most prolonged anti-proliferative potential (**Supp Fig. S7**). The concentrations of SN-38, M6620 and SRA-737 evaluated in these assays were lower than those clinically-achievable in patients based on the $C_{sd\text{-}max}$ described for these compounds (SN-38, $C_{sd\text{-}max}$ = 33 nM (25); SRA-737, $C_{sd\text{-}max}$ = 1.440 µM (26); M6620, $C_{sd\text{-}max}$ = 740 nM (27)), altogether supporting the relevance of our observations made with PARPi.

To further confirm the sensitivity of DSRCT to PARPi and ATRi, we sought to use a third, independent, biologically distinct and clinically relevant model. Since 3D and patient-derived models reportedly better recapitulate the clinical reality than 2D cultures or established cell line models (28–30), we sought to develop a new primary patient-derived organoid model of DSRCT. To do so, we first established a patient-derived xenograft (PDX) model from the primary peritoneal tumor of an 11-year-old male patient with DSRCT, and subsequently created a PDX-derived organoid (PDX-O), referred to as GR_13, in which we assessed the sensitivity to PARPi, ATRi and the combination of both agents (**Fig. 2E**, **Supp Fig. S8**). These experiments revealed cytotoxic effects of PARPi and ATRi monotherapies against GR_13 PDX-Os and confirmed the synergistic effects of their combination (Bliss independence score = 15.62; **Fig. 2F**, **Supp Fig. S9A-C**), albeit at higher concentrations, in line with the known heightened drug resistance of 3D models compared to 2D models (31). In line with PARP1 expression confirmed by western blot in GR_13 PDX-O (**Supp Fig. S8C**) and previous findings in the JN1 cell line (**Fig. 2C**, **Supp Fig. S6A**), this result confirmed our previous observations and the sensitivity of DSRCT to PARPi plus ATRi combinatorial strategy.

We next assessed the therapeutic potential of an ATRi plus PARPi combination *in vivo*, and evaluated the antitumor effect of PARPi talazoparib, ATRi M1774 or a combination of both agents in mice bearing established xenografts from the JN1 cell line (**Supp Fig. S10A**). Since JN1 tumors do not grow in nude mice, we used NOD scid gamma (NSG) mice that carry the *Prkdc*^{scid} mutation, which

confers exquisite sensitivity to DNA damaging agents and chronic exposure to ATRi. This required the use of a minimally toxic schedule of drug administration for a total maximum duration of 33 days. In this experiment, we found that compared to the drug vehicle, both talazoparib and M1774 monotherapies reduced tumor growth of JN1 xenografts (**Supp Fig. S10B, C**; $p < 0.001$, two-way ANOVA). The combination therapy further reduced tumor growth and caused tumor shrinkage (**Supp Fig. S10B-E**; median tumor volume: 151.5 mm^3 in vehicle arm, vs. 62.6 mm^3 in combination arm; $p < 0.0001$, two-way ANOVA). Altogether, these results suggested that the combination of PARPi and ATRi could act synergistically in DSRCT that express PARP1, both *in vitro* and *in vivo*.

Combination of PARP and ATR inhibitors elicits DNA damage, replication stress and genomic instability in DSRCT cells

To understand the molecular mechanisms underlying this vulnerability in DSRCT cells, we first sought to explore the known causes of PARPi and ATRi sensitivity, and assessed DNA damage, homologous recombination (HR) functionality, and replication stress. We found that exposure to PARPi and ATRi led to increased DNA damage, as assessed by immunofluorescence detection of γH2AX foci in JN1 and R cells (**Fig. 3A, B**). This effect was concentration-dependent (**Supp Fig. S11A, B**) and significantly enhanced in the context of PARPi plus ATRi combination using several clinical-grade agents, with γH2AX foci levels being similar to those induced by cisplatin (**Fig. 3A, B**). We further noted that γH2AX foci accumulation was (i) overall more pronounced in JN1 cells compared to R cells exposed to the combination therapy, and (ii) limited in

R cells exposed to PARPi as a monotherapy, consistent with the low PARP1 expression and limited PARPi sensitivity of this cell line. We next assessed HR function by quantifying the levels of RAD51 foci, and found that these were significantly increased in response to PARPi (**Fig. 3C, D**, **Supp Fig. S11C, D**) – but not ATRi monotherapy, in line with the current literature suggesting that ATR promotes RAD51 accumulation at DSBs (32). This effect was enhanced when both agents were combined, to a higher extent than cisplatin exposure (**Fig. 3C, D**). Altogether, these results suggested that DSRCT cells are HR proficient, and that their sensitivity to PARPi and ATRi does not result from a HR defect.

By mediating PARP1 trapping onto DNA, PARPi are known to increase reliance upon the ATR/CHK1 pathway due to increased stalled replication forks and a resultant replication stress (33). ATR is a master regulator of the DNA damage response, which coordinates cell cycle transitions with the DNA replication, DNA repair and apoptotic machineries to prevent the deleterious effects of replication stress. ATR activation leads to phosphorylation of CHK1 (p-CHK1) and other ATR effectors, which ultimately slows down origin firing, induces cell cycle arrest in response to DNA damage, and promotes stabilization and restart of stalled replication forks (34,35). We evaluated by western blot the phosphorylation of ATR and CHK1 and found increased p-CHK1 levels upon PARPi and ATRi exposure in JN1 and R cells (**Fig. 3E, F**, **Supp Fig. S11E**), suggesting an activation of the replication stress checkpoint. To further investigate the presence of ongoing replication stress, we evaluated the levels

of RPA2 phosphorylation (p-RPA2) and found increased p-RPA2 levels upon PARPi, ATRi and their combination. This was associated with increased DNA damage and apoptosis (as assessed by γH2AX and PARP1 cleavage, c-PARP, respectively; **Fig. 3E, F**, **Supp Fig. S11E**), consistent with our previous observations (**Fig. 3A, B**, **Supp Fig. S11A, B**).

To further assess the genomic consequences of PARPi plus ATRi combination in DSRCT, we measured levels of micronuclei – cytoplasmic chromosome fragments that arise during mitosis from lagging chromosomal DNA or chromatin bridges, as a result of unresolved DNA lesions. We found that the combination of PARPi and ATRi significantly increased the number of micronuclei in JN1 cells compared to the DMSO control or either of the corresponding monotherapies (**Fig. 3G, H**). A similar effect was observed in R cells (**Supp Fig. S11F**), although to a lesser extent, in line with their lower level of PARP1 expression. Altogether, these findings indicate that combined exposure of PARPi and ATRi elicits high levels of DNA damage, replication stress and micronuclei in DSRCT cells, in a context of functional HR repair.

EWS-WT1 is a determinant of sensitivity to PARP and ATR inhibitors in DSRCT

We next sought to explore whether the EWS-WT1 chimeric transcription factor was the cause of PARPi and ATRi sensitivity in DSRCT cells. Indeed, although the *EWSR1::WT1* fusion genes is the known driver of DSRCT, it remained possible that other alterations in DSRCT cells could cause the drug sensitivity

effects seen. For example, the t(11;22)(q13;q12) chromosomal translocation, beyond causing *EWS-WT1* fusion, also alters the chromosomal location of genes that flank either *EWSR1* or *WT1*.

To do so, we designed siRNAs targeting the specific breakpoints of the EWS-WT1 fusion in the JN1 and R cell lines, respectively (**Fig. 4A**; **Supp Fig. S1, S2**) and explored the effect of *EWS-WT1* silencing on the above-described phenotypes. We first assessed cell survival upon PARPi or ATRi exposure and observed that *EWS-WT1* silencing conferred increased resistance to both agent classes (**Fig. 4B-E**, **Supp Fig. S12A-D**), suggesting the existence of a common EWS-WT1-dependent mechanism driving sensitivity to both agents. Of note, silencing of *CCND1* – a direct target of EWS-WT1 (36) – conferred little increased resistance to PARPi or ATRi compared to *EWS-WT1* silencing in the JN1 cell line (**Supp Fig. S13**, **Supp Fig. S14A-D**), suggesting that the sensitivity to PARPi and ATRi induced by the fusion was, at least in part, independent from the role of EWS-WT1 in modulating *CCND1*. Similarly, and in line with this hypothesis, CDK1i-mediated cell cycle blockade failed to phenocopy the effects of siRNA-mediated *EWS-WT1* silencing towards increasing the resistance of DSRCT cells to either PARPi or ATRi (**Supp Fig. S14E-F**). This overall suggested that the sensitivity to PARPi and ATRi induced by the fusion was, at least in part, independent from its role in modulating *CCND1* expression and the cell cycle profile (**Supp Fig. S13**). We further found that levels of DNA damage induced by PARPi and ATRi were significantly reduced upon EWS-WT1 silencing, as assessed by immunofluorescence detection of γH2AX foci (**Fig. 4F, G**). To confirm the role of EWS-WT1 in PARPi

and ATRi-mediated effects, we next assessed ATR/CHK1 pathway activity by western blot and found that: (i) the PARPi-induced p-CHK1 response was abrogated upon *EWS-WT1* silencing; and (ii) the p-RPA2 and γH2AX responses elicited by PARPi plus ATRi combination were either reversed or significantly attenuated upon *EWS-WT1* silencing (**Fig. 4H, I**). These findings suggested that *EWS-WT1* is required for the sensitivity of DSRCT cells to PARPi, ATRi and their combination.

EWS-WT1 increases endogenous DNA replication stress and R-loops, which drive sensitivity to PARPi and ATRi

Because we observed that the sensitivity to PARPi and ATRi was EWS-WT1-dependent and since oncogenic transcription factors have been reported to increase replication stress (37), we next focused on replication forks and their functionality.

We first investigated replication fork progression upon silencing of *EWS-WT1* using the DNA fiber combing assay in the JN1 cell line. We found that *EWS-WT1* silencing caused a >30% increase in fork velocity (siCNTRL, 0.82 kb/min vs. siEWS-WT1, 1.1kb/min; $p < 0.0002$, Mann-Whitney U test; **Fig. 5A**) in the absence of drug exposure. Interestingly, this effect was not observed upon *CCND1* silencing (**Fig. 5A**), suggesting that EWS-WT1-induced reduction in replication fork velocity was, at least in part, independent from its effects in driving cell proliferation through the cell cycle (**Supp Fig. S13**). We next assessed replication fork progression upon PARPi and ATRi exposure in the JN1 cell line, and found that their combination decreased fork velocity (siCNTRL

DMSO, 0.82 kb/min vs. siCNTRL Tala + M4344, 0.58 kb /min; $p < 0.0001$, Mann-Whitney U test; **Fig. 5B**, **Supp Fig. S15A**), in line with these agents' mechanism of action and increased replication stress. This effect was partially rescued by *EWS-WT1* silencing (siCNTRL Tala + M4344, 0.7 kb/min vs. siEWS-WT1 Tala + M4344, 1.1 kb/min; $p < 0.0001$, Mann-Whitney U test; **Fig. 5B**). Altogether, these results suggested that EWS-WT1 expression in JN1 cells increases replication stress, which is further exacerbated by PARPi and ATRi exposure.

Since aberrant transcription factors not only cause replication stress but also enhance transcription, we next sought to assess R-loops. R-loops are three-stranded nucleic acid structures consisting of an RNA:DNA hybrid and a displaced non-hybridized single-stranded DNA, that form in the genome when an RNA strand invades double-stranded DNA within chromatin. R-loops naturally occur during replication and transcription, where they have important roles in regulating gene expression and chromatin structure. Their aberrant accumulation can also represent a threat to genomic stability, by causing increased replication stress and subsequent DNA damage (38–42).

We first assessed R-loop levels in DSRCT cells using RNA:DNA hybrid dot blotting with the S9.6 antibody on genomic DNA extracted from JN1 or R cells. We found that *EWS-WT1* silencing reduced endogenous R-loop levels in both JN1 and R cells (**Fig. 5C, D**), while *CCND1* silencing had no such effect (**Supp Fig. S15B**). We next compared R-loop levels in cells exposed to PARPi, ATRi or their combination in presence or absence of *EWS-WT1* silencing. This

601 revealed a significant accumulation of RNase H-sensitive R-loops in response
602 to the combination, which was (i) enhanced compared to either of the
603 corresponding monotherapies, and (ii) significantly attenuated in the context of
604 *EWS-WT1* silencing (**Fig. 5C, D**). To further explore the role of R-loops in
605 DSRCT cells, we constructed a JN1 cell line that stably expresses an
606 exogenous cDNA encoding *RNASEH1* – the main ribonuclease responsible for
607 R-loop degradation in humans – herein referred to as JN1-RNaseH1 (**Supp Fig.**
608 **S15C**). In contrast to our previous observations in the JN1 wildtype cell line (**Fig.**
609 **5A**), we noted that *EWS-WT1* silencing had no effect on replication fork velocity
610 in the JN1-RNaseH1 (**Fig. 5E**), suggesting that RNaseH1 overexpression might
611 counteract the replication stress resulting from EWS-WT1-driven R-loop burden.
612 Strikingly, dose-response survival assays of JN1 and JN1-RNaseH1 cells
613 exposed to various PARPi or ATRi monotherapies showed that RNase H1
614 overexpression conferred resistance to these inhibitors, supporting a role of R-
615 loops in driving PARPi and ATRi sensitivity in DSRCT cells (**Fig. 5F-I**; **Supp Fig.**
616 **S16**). Furthermore, we noted that: (i) the magnitude of this effect was similar to
617 that obtained when silencing EWS-WT1 in JN1 cells, and (ii) silencing *EWS-*
618 *WT1* conferred no further resistance to PARPi or ATRi in JN1-RNaseH1 cells
619 (**Fig. 5F-I**; **Supp Fig. S17**), supporting an epistasis between EWS-WT1
620 silencing and RNase H1 overexpression in driving resistance to PARPi and
621 ATRi. Altogether, these findings show that EWS-WT1 drives R-loop formation
622 and a resultant increased replication stress in DSRCT cells, which underlies
623 their sensitivity to PARPi and ATRi.
624

Combination of PARP and ATR inhibitors elicits cell-intrinsic immunity in DSRCT cell lines

The cyclic GMP-AMP synthase-stimulator of interferon genes (cGAS-STING) pathway is a component of the innate immune response: by acting as a sensor for cytosolic DNA, cGAS activates a signaling cascade involving STING trafficking, Tank-binding kinase 1 (TBK1) and interferon regulatory factor 3 (IRF3) phosphorylation, which culminates in a type I interferon response and the subsequent upregulation of interferon-stimulated genes (ISGs), such as *CCL5* and *CXCL10* (43). More recently, pharmacological manipulation of the cGAS-STING pathway has been proposed as a therapeutic strategy, notably in cancer to render tumors “immunologically hot” as a way to facilitate response to immunotherapies (44).

Based on recent reports, including ours, describing that PARPi and ATRi can trigger a cell-autonomous type I interferon response through activation the cGAS-STING pathway following micronuclei formation (41,45–50), we decided to explore the ability of PARPi and ATRi to elicit such response in DSRCT cells. We first observed a concentration-dependent increase in TBK1 and IRF3 phosphorylation upon PARPi and ATRi exposure in JN1 cells – an effect that was enhanced in the context of their combination (**Fig. 6A**). We next assessed downstream CCL5 and CXCL10 expression by RT-qPCR and found that these chemokines were increased by more than 20- and 5-fold respectively (**Fig. 6B, C**) upon combination therapy. This was further accompanied by a concentration-dependent increase in programmed death-ligand 1 (PD-L1) cell-surface expression, as assessed by flow cytometry (**Fig. 6D**). Together with our

previous observation that the PARPi plus ATRi combination induces micronuclei formation (**Fig. 3G, H**; **Supp Fig. S11F**), this data suggests that a cell-autonomous cGAS-STING-mediated type I interferon response is activated in DSRCT cells as a result of PARPi and ATRi exposure. We next investigated the role of EWS-WT1 in such response, and found that *EWS-WT1* silencing attenuated all of the above phenotypes, including TBK1 and IRF3 phosphorylation (**Fig. 6E**), CCL5 and CXCL10 upregulation (**Fig. 6F-G**) as well as PD-L1 cell-surface expression (**Fig. 6H**). Altogether, these results indicate that PARPi and ATRi elicit a type I interferon response in DSRCT cells that is dependent upon EWS-WT1 expression.

Discussion

DSRCT is an extremely aggressive malignancy with very limited therapeutic options. Here, we show that preclinical models of DSRCT are selectively sensitive to clinical PARP and ATR inhibitors (PARPi, ATRi). The use of functional genomics allowed us to propose a model whereby these genetic vulnerabilities are mediated by increased EWS-WT1-dependent replication stress and R-loop formation, which results in cGAS/STING pathway activation and a cell-autonomous type I interferon response (**Fig. 6I**), opening new therapeutic avenues to increase immunogenicity of this genetically simple, immune-cold disease.

To our knowledge, our work represents the first report of the selective sensitivity of DSRCT cells to ATRi, and of the involvement of EWS-WT1-dependent R-loop burden in this vulnerability. Our work specifically underlines the translational potential of combining PARPi and ATRi in DSRCT, a combination that is currently evaluated in multiple clinical trials, including in children (NCT02813135). Previous literature has suggested a sensitivity of DSRCT to PARPi in combination with the alkylating agent temozolomide, following the observation of a high level of PARP1 and SLFN11 expression in DSRCT (20). Our analysis of 29 and 16 tumor samples by RNA-Seq and IHC confirms these findings, thereby reinforcing the potential of using such DNA damage response inhibitors in the treatment of patients with DSRCT. Still, our observation that some tumors do not express PARP1 – a major mechanism of resistance to PARPi (21,51) – highlights the need for careful molecular selection and

verification of adequate PARP1 expression prior to treatment orientation.

The potential for using CHK1 inhibitors (CHK1i), such as prexasertib, has also been reported in preclinical models of DSRCT (52), and further evaluated in a clinical trial in combination with irinotecan (53) (NCT04095221). In that latter, 6/19 (32%) and 9/19 (47%) patients showed partial response and stable disease as best response, respectively. The trial met its primary endpoint, supporting further investigation of this combination. Data regarding the PARPi plus ATRi combination in DSRCT are much scarcer for now: one heavily pretreated patient, who received the PARPi olaparib plus ATRi AZD6738 combination as part of the eSMART trial (NCT02813135), presented stable disease for 4 months on study (15). Additional data from this trial are eagerly awaited, to better evaluate the potential of this combination in patients with DSRCT. Since CHK1i and ATRi both act on the G_2/M cell cycle checkpoint, we can anticipate that their mechanism of action is partially overlapping. Based on available clinical data, the PARPi plus ATRi combination may have a better tolerability profile than the CHK1i plus irinotecan combination, notably with regards to fatigue and cytopenias (15,53,54). In the former combination, the oral administration of both drugs also represents an important difference between the two regimens, which may offer the advantage of a higher flexibility in scheduling and dosage adaptations. However, it also represents a limitation for patients who have peritoneal disease – and are therefore at risk of malabsorption, occlusion, etc. – and PARPi have shown disappointing efficacy in pediatric malignancies so far. In this context, we can hope that the use of last

generation potent PARP1-selective inhibitors (e.g. AZD5305) will allow to enhance PARPi efficacy while limiting hematological toxicity.

DSRCT is related to the group of small round cell sarcomas (SRCS), of which Ewing's sarcoma is the prototypic EWS-FLI1-driven disease. PARP1 inhibition has initially been proposed as a therapeutic strategy in Ewing's sarcoma, following the identification of an interaction between PARP1 and the fusion transcripts which potentiated DNA damage (55). EWS-FLI1 was subsequently reported to increase the R-loop burden and disable BRCA1-dependent homologous recombination. Such "BRCAness" phenotype was not observed in our study, where we could detect adequate RAD51 foci formation in DSRCT cells exposed to PARPi. Thus far, PARPi have shown disappointing efficacy in patients with heavily pre-treated Ewing's sarcoma (reviewed in Pearson et al (56)). A few isolated responses have been observed, which deserve further molecular exploration to identify which clinically-relevant biomarkers drive sensitivity in this population. Based on these results, the most recent consensus expert guidelines from the multi-stakeholder Pediatric Strategy Forum on DNA repair (ACCELERATE and European Medicines Agency, with participation of the Food and Drug Administration), recommended to assess CHK1i and ATRi as a high priority, and PARPi only in combination with the latter (56). The synergy observed preclinically upon combination of PARPi and ATRi in the JN1 cell line (**Fig. 2C**) and GR_13 PDX-O model (**Fig. 2F**) also supports the latter approach. Beyond SRCS, trabectedin – a cytotoxic drug used in routine sarcoma treatment and which is known to induce R-loops (57) – has been

combined with PARPi in various soft-tissue sarcomas in the TOMAS trial (58). Unsurprisingly, these agents could not be used at full dose when combined, but activity (7/50 patients enrolled with PR) supported the evaluation of this combination in an ongoing Phase II trial (NCT03838744). Although this combination is very poorly tolerated as compared to the PARPi plus ATRi combination, authors identified high PARP1 expression as well as an 8-genes signature (including DNA damage response genes such as *SLFN11*, *ATM* and *BLM*) as predictors of better outcome on trabectedin plus PARPi (59). The latter may also be relevant to the PARPi plus ATRi combination.

We finally found that PARPi and ATRi trigger a cell-autonomous cGAS-STING / type I interferon response and PD-L1 upregulation in DSRCT cells. This immunomodulatory effect of DNA repair inhibitors could be exploited to increase the immunogenicity of DSRCT – which are traditionally devoid of T-cells in the tumor microenvironment – by attracting T-cells within the tumor and favoring sensitivity to anti-PD-1 therapy. Such effect of PARPi and ATRi has been reported in other preclinical models with high replication stress (reviewed in Chabanon et al (60)), as well as in clinical studies evaluating ATRi, notably in non-small cell lung cancer (NSCLC) and melanoma where they can potentiate, or revert resistance to anti-PD-L1, respectively (61–63). For example, translational studies performed in the HUDSON phase II trial showed that the ATRi AZD6738 could both induce inflammatory- and interferon-associated signatures, and decrease exhausted CD8+ T-cells in the blood of patients with NSCLC (62). Still, whether such effects are only observed in traditionally

immunogenic diseases, such as NSCLC or melanoma, or also operate in DSRCT, remains to be assessed.

We should still highlight several limitations to our observations. First, we only had access to a limited number of models. Indeed, DSRCT is an ultra-rare disease (frequency < 1/1M) and cell lines models are challenging to create, probably because the desmoplastic microenvironment of this tumor type also favors cancer cell growth. In this study, we therefore created two previously unpublished models (one PDX-derived cell line and one PDX-derived organoid), which complemented the previously established JN1 cell line. Still, revalidation in additional models would ideally be required. Second, the difference in PARP1 expression between our models led to discrepant observations, notably in terms of synergistic or additive cytotoxic effects of the PARPi plus ATRi combination, in which PARP1 expression and trapping plays a crucial role (21,51). Our characterization of PARP1 expression and PARylation in DSRCT patients' tumors shows that PARP1 is expressed and active in the vast majority of cases – in line with previous independent results (20), thereby supporting clinical activity of PARPi in this patient population. Still, other determinants of PARPi and ATRi sensitivity, such as SLFN11 expression and replication stress levels, should also be considered, and the clinical applicability of our findings therefore remains unknown. Finally, we faced technical difficulties in assessing long-term efficacy of the PARPi plus ATRi combination *in vivo*, owing to the systemic toxicity of ATRi in NSG mice caused by their constitutive *Prkdc*^{scid} mutation, and the impossibility to grow DSRCT xenografts in nude mice, which led us to

779 prematurely stop our experiments. If recent clinical trial results show that PARPi
780 and ATRi can be safely combined in adult and pediatric patients, the efficacy /
781 toxicity profile of such combination may need to be compared to that of other
782 regimens that also act on the DNA damage response and replication stress
783 (e.g., CHK1i and irinotecan combinations; NCT04095221 (52,53)), to better
784 define its role in the therapeutic armamentarium. Despite these limitations, we
785 believe our study may have translational utility and clinical impact in DSRCT, a
786 disease where very few therapeutic options and no precision medicine
787 approach are available.
788
789 In conclusion, our findings shed light on EWS-WT1-associated genetic
790 vulnerabilities in DSRCT and provide rationale for evaluating PARPi in
791 combination with ATRi in this deadly disease. Since the replication stress- and
792 R-loop-dependency of this phenotype may also operate in other, more frequent,
793 transcription factor-driven sarcomas – such as Ewing's sarcoma or synovial
794 sarcoma, we hope that this will favor the development of basket studies
795 enrolling multiple biomarker-selected sarcomas and allow patients to access
796 these therapies despite the rarity of their disease.

Authors' Contribution

Conception and design: AKK, MML, CA, RMC, SPV.

Development of methodology: AKK, MML, CA, MBC, SM, CJL, RMC, SPV.

Acquisition of data (provided animals, provided facilities, etc.): AKK, MML, CA, NH, MBC, CN, MG, TE, ND, LB, FS, RB, AL, ARM, LCD, MD, ES, OM, GP, AG, RMC.

Analysis and interpretation of data: AKK, MML, CA, NH, MBC, CN, MG, TE, ND, AL, ARM, LCD, MD, ES, AG, RMC.

Writing, review, and/or revision of the manuscript: All authors.

Administrative, technical, or material support: MBC, LCD, JS, SM, AZ, RMC, CJL, SPV.

Study supervision: RMC, SPV.

Acknowledgements

We dedicate this research to patients and their families. We thank patients and families for their donations to the Gustave Roussy Sarcoma Tumor Board and Research program, Gustave Roussy Sarcoma Donors, Association “Un élan pour Lucas” and Family L, whose donations have been instrumental in allowing us to pursue this project. AKK was funded by ESMO fellowship and donations via the Gustave Roussy Sarcoma Committee; CA was funded by a Fondation pour la Recherche Médicale (FRM) PhD fellowship (ECO202206015528); RMC received award funding from Association Ruban Rose, Fondation Bettencourt-Schueller, Institut Servier, Fondation des Treilles and Cancéropôle Ile-De-France.

This work was also funded by programme grants to SPV from Société Française Cancers Enfant / Imagine for Margo, Cancéropôle Ile-de-France (Recherche et Innovation en Cancérologie-RIC-01-IGR and 2017-1-EMERG-72), Fondation ARC (PGA1-RF20190208576), European Research Council ERC (TargetSWitch 101077864), INSERM ATIP-Avenir / La Ligue Contre le Cancer 2018; as well as programme grants to Gustave Roussy from Institut National du Cancer (INCa-DGOS-Inserm_12551 SIRIC2 and INCa-DGOS-Inserm-ITMO Cancer_18002 SIRIC EpiCURE).

We also thank FIGHT KIDS CANCER (FKC) Representatives KickCancer, Imagine for Margo, Foundation Kriibskrank Kanner and CRIS Cancer Foundation for awarding the 2024 FIGHT KIDS CANCER & St. Baldrick’s Foundation Arceci Innovation Award to SPV. The independent selection

process of this Innovation Award, funded by FKC, was administered by the St Baldrick's Foundation.

Work carried out in the lab of CJL was funded via a CRUK Programme Grant.

RMC and SPV thank Dr. M Gary Bobo and Dr. L Ali for having performed some orthogonal validation experiments not included in the final manuscript.

AL, ARM and JS thank the Kelly Turner Foundation, the Tom Bowdidge Youth Cancer Foundation and RobsARTTT for their support.

References

1. Subbiah V, Lamhamedi-Cherradi S-E, Cuglievan B, Menegaz BA, Camacho P, Huh W, et al. Multimodality Treatment of Desmoplastic Small Round Cell Tumor: Chemotherapy and Complete Cytoreductive Surgery Improve Patient Survival. Clin Cancer Res Off J Am Assoc Cancer Res. 2018;24:4865–73.

2. Cidre-Aranaz F, Watson S, Amatruda JF, Nakamura T, Delattre O, de Alava E, et al. Small round cell sarcomas. Nat Rev Dis Primer. 2022;8:66.

3. Mello CA, Campos FAB, Santos TG, Silva MLG, Torrezan GT, Costa FD, et al. Desmoplastic Small Round Cell Tumor: A Review of Main Molecular Abnormalities and Emerging Therapy. Cancers. 2021;13:498.

4. Chow WA, Yee J-K, Tsark W, Wu X, Qin H, Guan M, et al. Recurrent secondary genomic alterations in desmoplastic small round cell tumors. BMC Med Genet. 2020;21:101.

5. Slotkin EK, Bowman AS, Levine MF, Dela Cruz F, Coutinho DF, Sanchez GI, et al. Comprehensive Molecular Profiling of Desmoplastic Small Round Cell Tumor. Mol Cancer Res MCR. 2021;19:1146–55.

6. Wu C-C, Beird HC, Lamhamedi-Cherradi S-E, Soeung M, Ingram D, Truong DD, et al. Multi-site desmoplastic small round cell tumors are genetically related and immune-cold. NPJ Precis Oncol. 2022;6:21.

7. Devecchi A, De Cecco L, Dugo M, Penso D, Dagrada G, Brich S, et al. The genomics of desmoplastic small round cell tumor reveals the deregulation of genes related to DNA damage response, epithelial-mesenchymal transition, and immune response. Cancer Commun Lond Engl. 2018;38:70.

8. Vanoli F, Tomishima M, Feng W, Lamribet K, Babin L, Brunet E, et al. CRISPR-Cas9-guided oncogenic chromosomal translocations with conditional fusion protein expression in human mesenchymal cells. Proc Natl Acad Sci U S A. 2017;114:3696–701.

9. Gedminas JM, Chasse MH, McBrairty M, Beddows I, Kitchen-Goosen SM, Grohar PJ. Desmoplastic small round cell tumor is dependent on the EWS-

WT1 transcription factor. Oncogenesis. 2020;9:41.

10. Bushweller JH. Targeting transcription factors in cancer - from undruggable to reality. Nat Rev Cancer. 2019;19:611–24.

11. Nishio J, Iwasaki H, Ishiguro M, Ohjimi Y, Fujita C, Yanai F, et al. Establishment and characterization of a novel human desmoplastic small round cell tumor cell line, JN-DSRCT-1. Lab Investig J Tech Methods Pathol. 2002;82:1175–82.

12. Holme H, Gulati A, Brough R, Fleuren EDG, Bajrami I, Campbell J, et al. Chemosensitivity profiling of osteosarcoma tumour cell lines identifies a model of BRCAness. Sci Rep. 2018;8:10614.

13. Bigot L, Sabio J, Poiraudeau L, Annereau M, Menssouri N, Helissey C, et al. Development of Novel Models of Aggressive Variants of Castration-resistant Prostate Cancer. Eur Urol Oncol. 2023;S2588-9311(23)00226-2.

14. Bialic M, Coulon V, Drac M, Gostan T, Schwob E. Analyzing the dynamics of DNA replication in mammalian cells using DNA combing. Methods Mol Biol. 2015;1300:67–78.

15. Gatz SA, Simón ARS, Archambaud B, Abbou S, Cleirec M, Leruste A, et al. Abstract CT019: Phase I/II study of the PARP inhibitor olaparib and ATR inhibitor ceralasertib in children with advanced malignancies: Arm N of the AcSé-ESMART trial. Cancer Res. 2023;83:CT019.

16. Goldstein MJ, Peters M, Weber BL, Davis CB. Optimizing the Therapeutic Window of Targeted Drugs in Oncology: Potency-Guided First-in-Human Studies. Clin Transl Sci. 2021;14:536–43.

17. Yap TA, Krebs MG, Postel-Vinay S, El-Khouiery A, Soria J-C, Lopez J, et al. Ceralasertib (AZD6738), an Oral ATR Kinase Inhibitor, in Combination with Carboplatin in Patients with Advanced Solid Tumors: A Phase I Study. Clin Cancer Res. 2021;

18. Burris HA, Berlin J, Arkenau T, Cote GM, Lolkema MP, Ferrer-Playan J, et al. A phase I study of ATR inhibitor gartisertib (M4344) as a single agent and in combination with carboplatin in patients with advanced solid

tumours. Br J Cancer. 2024;130:1131–40.

19. Tlemsani C, Heske CM, Elloumi F, Pongor L, Khandagale P, Varma S, et al. Sarcoma_CellminerCDB: A tool to interrogate the genomic and functional characteristics of a comprehensive collection of sarcoma cell lines. iScience [Internet]. Elsevier; 2024 [cited 2024 Jun 28];27. Available from: https://www.cell.com/iscience/abstract/S2589-0042(24)01003-4

20. van Erp AEM, van Houdt L, Hillebrandt-Roeffen MHS, van Bree NFHN, Flucke UE, Mentzel T, et al. Olaparib and temozolomide in desmoplastic small round cell tumors: a promising combination in vitro and in vivo. J Cancer Res Clin Oncol. 2020;146:1659–70.

21. Pettitt SJ, Krastev DB, Brandsma I, Dréan A, Song F, Aleksandrov R, et al. Genome-wide and high-density CRISPR-Cas9 screens identify point mutations in PARP1 causing PARP inhibitor resistance. Nat Commun. 2018;9:1849.

22. Murai J, Huang SN, Das BB, Renaud A, Zhang Y, Doroshow JH, et al. Trapping of PARP1 and PARP2 by Clinical PARP Inhibitors. Cancer Res. 2012;72:5588–99.

23. Pommier Y, O'Connor MJ, de Bono J. Laying a trap to kill cancer cells: PARP inhibitors and their mechanisms of action. Sci Transl Med. 2016;8:362ps17.

24. Henon C, Vibert J, Eychenne T, Gruel N, Colmet-Daage L, Ngo C, et al. Single-cell multiomics profiling reveals heterogeneous transcriptional programs and microenvironment in DSRCTs. Cell Rep Med. 2024;5:101582.

25. Bomgaars LR, Bernstein M, Krailo M, Kadota R, Das S, Chen Z, et al. Phase II trial of irinotecan in children with refractory solid tumors: a Children's Oncology Group Study. J Clin Oncol Off J Am Soc Clin Oncol. 2007;25:4622–7.

26. Banerji U, Plummer ER, Moreno V, Ang JE, Quinton A, Drew Y, et al. A phase I/II first-in-human trial of oral SRA737 (a Chk1 inhibitor) given in combination with low-dose gemcitabine in subjects with advanced cancer.

J Clin Oncol. Wolters Kluwer; 2019;37:3095–3095.

27. Kiesel BF, Scemama J, Parise RA, Villaruz L, Iffland A, Doyle A, et al. LC-MS/MS assay for the quantitation of the ATR kinase inhibitor VX-970 in human plasma. J Pharm Biomed Anal. 2017;146:244–50.

28. Zanoni M, Piccinini F, Arienti C, Zamagni A, Santi S, Polico R, et al. 3D tumor spheroid models for in vitro therapeutic screening: a systematic approach to enhance the biological relevance of data obtained. Sci Rep. Nature Publishing Group; 2016;6:19103.

29. Bleijs M, van de Wetering M, Clevers H, Drost J. Xenograft and organoid model systems in cancer research. EMBO J. John Wiley & Sons, Ltd; 2019;38:e101654.

30. Magrath JW, Kang H-J, Hartono A, Espinosa-Cotton M, Somwar R, Ladanyi M, et al. Desmoplastic small round cell tumor cancer stem cell-like cells resist chemotherapy but remain dependent on the EWSR1-WT1 oncoprotein. Front Cell Dev Biol. 2022;10:1048709.

31. Horning JL, Sahoo SK, Vijayaraghavalu S, Dimitrijevic S, Vasir JK, Jain TK, et al. 3-D tumor model for in vitro evaluation of anticancer drugs. Mol Pharm. 2008;5:849–62.

32. Buisson R, Niraj J, Rodrigue A, Ho CK, Kreuzer J, Foo TK, et al. Coupling of Homologous Recombination and the Checkpoint by ATR. Mol Cell. 2017;65:336–46.

33. Lord CJ, Ashworth A. PARP inhibitors: Synthetic lethality in the clinic. Science. 2017;355:1152–8.

34. Groelly FJ, Fawkes M, Dagg RA, Blackford AN, Tarsounas M. Targeting DNA damage response pathways in cancer. Nat Rev Cancer. 2023;23:78–94.

35. da Costa AABA, Chowdhury D, Shapiro GI, D'Andrea AD, Konstantinopoulos PA. Targeting replication stress in cancer therapy. Nat Rev Drug Discov. 2023;22:38–58.

36. Liu J, Nau MM, Yeh JC, Allegra CJ, Chu E, Wright JJ. Molecular heterogeneity and function of EWS-WT1 fusion transcripts in desmoplastic small round cell tumors. Clin Cancer Res Off J Am Assoc Cancer Res. 2000;6:3522–9.

37. Gorthi A, Romero JC, Loranc E, Cao L, Lawrence LA, Goodale E, et al. EWS-FLI1 increases transcription to cause R-Loops and block BRCA1 repair in Ewing sarcoma. Nature. 2018;555:387–91.

38. Petermann E, Lan L, Zou L. Sources, resolution and physiological relevance of R-loops and RNA-DNA hybrids. Nat Rev Mol Cell Biol. 2022;23:521–40.

39. Kotsantis P, Silva LM, Irmscher S, Jones RM, Folkes L, Gromak N, et al. Increased global transcription activity as a mechanism of replication stress in cancer. Nat Commun. 2016;7:13087.

40. Groelly FJ, Dagg RA, Petropoulos M, Rossetti GG, Prasad B, Panagopoulos A, et al. Mitotic DNA synthesis is caused by transcription-replication conflicts in BRCA2-deficient cells. Mol Cell. 2022;82:3382-3397.e7.

41. Chabanon RM, Morel D, Eychenne T, Colmet-Daage L, Bajrami I, Dorvault N, et al. PBRM1 Deficiency Confers Synthetic Lethality to DNA Repair Inhibitors in Cancer. Cancer Res. 2021;81:2888–902.

42. Bayona-Feliu A, Barroso S, Muñoz S, Aguilera A. The SWI/SNF chromatin remodeling complex helps resolve R-loop-mediated transcription-replication conflicts. Nat Genet. 2021;53:1050–63.

43. Motwani M, Pesiridis S, Fitzgerald KA. DNA sensing by the cGAS-STING pathway in health and disease. Nat Rev Genet. 2019;20:657–74.

44. Samson N, Ablasser A. The cGAS-STING pathway and cancer. Nat Cancer. 2022;3:1452–63.

45. Chabanon RM, Muirhead G, Krastev DB, Adam J, Morel D, Garrido M, et al. PARP inhibition enhances tumor cell–intrinsic immunity in ERCC1-deficient non–small cell lung cancer. J Clin Invest. 2019;129:1211–28.

46. Pantelidou C, Sonzogni O, Taveira MDO, Mehta AK, Kothari A, Wang D, et al. PARP inhibitor efficacy depends on CD8+ T-cell recruitment via intratumoral STING pathway activation in BRCA-deficient models of triple-negative breast cancer. Cancer Discov. 2019;9:722–37.

47. Ding L, Kim HJ, Wang Q, Kearns M, Jiang T, Ohlson CE, et al. PARP Inhibition Elicits STING-Dependent Antitumor Immunity in Brca1-Deficient Ovarian Cancer. Cell Rep. 2018;25:2972–80.

48. Reisländer T, Lombardi EP, Groelly FJ, Miar A, Porru M, Di Vito S, et al. BRCA2 abrogation triggers innate immune responses potentiated by treatment with PARP inhibitors. Nat Commun. 2019;10:3143–3143.

49. Wang Z, Sun K, Xiao Y, Feng B, Mikule K, Ma XY, et al. Niraparib activates interferon signaling and potentiates anti-PD-1 antibody efficacy in tumor models. Sci Rep. 2019;9:1853–1853.

50. Feng X, Tubbs A, Zhang C, Tang M, Sridharan S, Wang C, et al. ATR inhibition potentiates ionizing radiation-induced interferon response via cytosolic nucleic acid-sensing pathways. EMBO J. 2020;39:e104036–e104036.

51. Pettitt SJ, Rehman FL, Bajrami I, Brough R, Wallberg F, Kozarewa I, et al. A genetic screen using the PiggyBac transposon in haploid cells identifies Parp1 as a mediator of olaparib toxicity. PloS One. 2013;8:e61520.

52. Lowery CD, Dowless M, Renschler M, Blosser W, VanWye AB, Stephens JR, et al. Broad Spectrum Activity of the Checkpoint Kinase 1 Inhibitor Prexasertib as a Single Agent or Chemopotentiator Across a Range of Preclinical Pediatric Tumor Models. Clin Cancer Res Off J Am Assoc Cancer Res. 2019;25:2278–89.

53. Slotkin EK, Mauguen A, Ortiz MV, Dela Cruz FS, O'Donohue T, Kinnaman MD, et al. A phase I/II study of prexasertib in combination with irinotecan in patients with relapsed/refractory desmoplastic small round cell tumor and rhabdomyosarcoma. J Clin Oncol. Wolters Kluwer; 2022;40:11503–11503.

54. Mahdi H, Hafez N, Doroshow D, Sohal D, Keedy V, Do KT, et al. Ceralasertib-Mediated ATR Inhibition Combined With Olaparib in

Advanced Cancers Harboring DNA Damage Response and Repair Alterations (Olaparib Combinations). JCO Precis Oncol. 2021;5:PO.20.00439.

55. Brenner JC, Feng FY, Han S, Patel S, Goyal SV, Bou-Maroun LM, et al. PARP-1 inhibition as a targeted strategy to treat Ewing's sarcoma. Cancer Res. 2012;72:1608–13.

56. Pearson ADJ, Zwaan CM, Kolb EA, Karres D, Guillot J, Kim SY, et al. Paediatric Strategy Forum for medicinal product development for acute myeloid leukaemia in children and adolescents: ACCELERATE in collaboration with the European Medicines Agency with participation of the Food and Drug Administration. Eur J Cancer Oxf Engl 1990. 2020;136:116–29.

57. Tumini E, Herrera-Moyano E, San Martín-Alonso M, Barroso S, Galmarini CM, Aguilera A. The Antitumor Drugs Trabectedin and Lurbinectedin Induce Transcription-Dependent Replication Stress and Genome Instability. Mol Cancer Res MCR. 2019;17:773–82.

58. Grignani G, D'Ambrosio L, Pignochino Y, Palmerini E, Zucchetti M, Boccone P, et al. Trabectedin and olaparib in patients with advanced and non-resectable bone and soft-tissue sarcomas (TOMAS): an open-label, phase 1b study from the Italian Sarcoma Group. Lancet Oncol. 2018;19:1360–71.

59. Merlini A, Centomo ML, Ferrero G, Chiabotto G, Miglio U, Berrino E, et al. DNA damage response and repair genes in advanced bone and soft tissue sarcomas: An 8-gene signature as a candidate predictive biomarker of response to trabectedin and olaparib combination. Front Oncol. 2022;12:844250.

60. Chabanon RM, Rouanne M, Lord CJ, Soria J-C, Pasero P, Postel-Vinay S. Targeting the DNA damage response in immuno-oncology: developments and opportunities. Nat Rev Cancer. 2021;21:701–17.

61. Besse B, Awad MM, Forde PM, Thomas M, Goss G, Aronson B, et al. OA15.05 HUDSON: An Open-Label, Multi-Drug, Biomarker-Directed Phase

2 Study in NSCLC Patients Who Progressed on Anti-PD-(L)1 Therapy. J Thorac Oncol. 2022;17:S41–2.

62. Iyer S, Conway J, Russell D, Reddy A, Cosaert J, Barry S, et al. Abstract CT039: Immunomodulatory effects of ceralasertib in combination with durvalumab in patients with NSCLC and progression on anti-PD-(L)1 treatment (HUDSON, NCT03334617). Cancer Res. 2023;83:CT039.

63. Kim R, Kwon M, An M, Kim ST, Smith SA, Loembé AB, et al. Phase II study of ceralasertib (AZD6738) in combination with durvalumab in patients with advanced/metastatic melanoma who have failed prior anti-PD-1 therapy. Ann Oncol Off J Eur Soc Med Oncol. 2022;33:193–203.

Figure Legends

Figure 1. A small-molecule inhibitor and drug screen identifies PARP and ATR inhibitors as candidate therapies for DSRCT. **A.** Schematic illustration of the workflow of small-molecule inhibitor and drug screen performed on the JN-DSRCT-1 (JN1) cell line. **B.** Waterfall plot displaying the difference in AUC between the JN1 cell line (AUC_{JN1}) and the panel of 92 cell lines used for comparison (AUC_{median}) for the 79 evaluated small-molecule inhibitors or drugs. PARP inhibitors are highlighted in red, ATR inhibitors in blue, and conventional cytotoxic agents in green. AUC, Area Under the Curve. **C-F.** Dose-response survival curves of the DSRCT cell lines JN1 and R, and the A673 (Ewing sarcoma) and SaOS-2 (osteosarcoma) cell lines exposed to talazoparib (C), M4344 (D), olaparib (E), or AZD6738 (F) for 7 days. Mean ± SD; *n* = 3. **G, H.** Violin plots showing the relative sensitivity (log_2 fold-change of cell viability) of cell lines exposed to the PARP inhibitor talazoparib (G) or olaparib (H) after a single-dose exposure at 2.5µM for 5 days in the DepMap database (Prism Repurposing 23Q2), in comparison with that of the JN1 and R cell lines. JN1 and R cell lines sensitivities were extrapolated from the survival assays presented in C and D; surviving fractions were calculated at 2.5µM and log_2 transformed. Ewing Sarcoma cell lines (n=23): RDES, A673, SKES1, CADOES1, EWS502, MHHES1, EW8, A673STAG2KO16, A673STAG2KO45, A673STAG2NT14, A673STAG2NT23, CBAGPN, CHLA10, SKNEP1, SKPNDW, TC32; Osteosarcoma cell lines (n=5): G292CLONEA141B1, MG63, U2OS,

HOS, SJSA1; Soft-tissue sarcoma cell lines (n=7): S117, TE617T, HT1080, HS729, RD, RKN, RH30, including rhabdomyosarcoma (n=4), leiomyosarcoma (n=1), fibrosarcoma (n=1) and NOS sarcoma cell lines (n=1), respectively. The BRCA1/2-mutant IGROV1 ovarian cancer cell line and BRCA1-mutant MDA-MB-436 breast cancer cell line were used as positive controls for sensitivity to PARP inhibitors.

Figure 2. PARP and ATR inhibitors have synergistic cytotoxic effects in models of DSRCT with high PARP1 expression. A, B. PARP1 expression (A) and PARylation levels (B) as assessed by immunohistochemistry in a cohort of 16 DSRCT samples, compared with those of the JN1 and R cell lines (PARP1 and PAR expression are shown as H-scores). Representative cases (PARP1-high vs. -low tumors; PAR-high vs. -low tumors) are shown to the right, compared with JN1 and R cells. **C, D.** Surface plots of Bliss independence scores calculated for the talazoparib – M4344 combination in JN1 (C) and R (D) cell lines at 7 days. **E.** GR_13-PDX-O model was established from the primary peritoneal tumor of a patient with DSRCT, with confirmation of EWS-WT1 fusion by FISH and WT1-Cter IHC. **F.** Surface plot of Bliss independence score calculated for the talazoparib – M4344 combination in the GR_13 PDX-O at 7 days. The associated dose-response matrix is shown to the right. Mean ± SD, n=3. Surface plots: the x- and y-axes values indicate drug concentrations, and the z-axis values the associated synergy score; score < -10, antagonistic interaction; score = 0, absence of interaction; score > 10, synergistic interaction.

Figure 3. PARP and ATR inhibitors elicits DNA damage, replication stress and genomic instability in DSRCT cells.

A-D. Quantification of γH2AX (A, B) or RAD51 foci (C, D) in JN1 (A, C) or R cells (B, D) exposed to DMSO control, PARPi talazoparib, ATRi M4344, or a combination of both for 72 h. Cisplatin was used as a positive control. A minimum of 500 nuclei were analyzed per condition. Violin plots show the absolute number of foci per nucleus. Thick line, median; thin lines, lower and upper quartiles; two-way ANOVA and *post hoc* Dunn's test. **E, F.** Western blot of pCHK1, CHK1, pRPA2, RPA2, γH2AX, H2AX, and cleaved-PARP1 (cPARP) in JN1 (E) or R (F) cells exposed to DMSO control, PARPi talazoparib or olaparib, ATRi M4344 or AZD6738, or a combination of both for 48 h. **G, H.** Representative immunofluorescence images (G) and quantification of micronuclei-positive cells (H) in JN1 cells exposed to DMSO control, PARPi talazoparib, ATRi M4344, or a combination of both for 72 h. A minimum of 500 cells were analyzed per condition. Mean ± SD; $n = 3$; one-way ANOVA and *post hoc* Dunn's test. Arrows indicate micronuclei. Scale bar, 20μm.

Figure 4. EWS-WT1 is a determinant of DSRCT cells' sensitivity to PARPi and ATRi. **A.** Western blot of EWS-WT1 in JN1 and R cells transfected with either siCNTRL or siEWS-WT1. Whole-cell lysates were generated 48h post-transfection. **B-E.** Dose-response survival curves of JN1 or R cells exposed to PARPi talazoparib (B, C) or ATRi M4344 (D, E) for 7 days in presence or absence of siRNA-mediated silencing of EWS-WT1. Mean ± SD; $n = 3$. **F, G**.

Quantification of γH2AX in JN1 cells exposed to DMSO control, PARPi talazoparib, ATRi M4344, or a combination of both for 72 h, in presence or absence of siRNA-mediated silencing of EWS-WT1. Cisplatin was used as a positive control. A minimum of 500 nuclei were analyzed per condition. Violin plots show the absolute number of foci per nucleus. Thick line, median; thin lines, lower and upper quartiles; two-way ANOVA and *post hoc* Dunn's test. **H, I.** Western blot of pCHK1, CHK1, pRPA2, RPA2, γH2AX, H2AX, and EWS-WT1 in JN1 (I) or R cells (J) exposed to DMSO control, PARPi talazoparib, ATRi M4344, or a combination of both for 48 h, in presence or absence of siRNA-mediated silencing of EWS-WT1.

Figure 5. EWS-WT1 drives enhanced DNA replication stress and R-loops, which contribute to DSRCT cells' sensitivity to PARPi and ATRi. **A**. Assessment of replication fork speed (kb/min) in JN1 cells subjected to siRNA-mediated silencing of EWS-WT1 or CCND1. A minimum of 50 forks were analyzed per condition. Mean ± SD, each dot represents a single replication fork; *n* = 2, one-way ANOVA and *post hoc* Dunnett's test. **B.** Assessment of replication fork speed (kb/min) in JN1 cells exposed to DMSO control, or a combination of PARPi talazoparib and ATRi M4344 for 6 h, in presence or absence of siRNA-mediated silencing of EWS-WT1. A minimum of 50 forks were analyzed per condition. Mean ± SD, each dot represents a single replication fork; *n* = 2, two-way ANOVA and *post hoc* Šídák's test. **C, D.** DNA:RNA hybrid dot blot of genomic DNA extracted from JN1 (C) or R cells (D) exposed to PARPi talazoparib, ATRi M4344 or a combination of both in

presence or absence of siRNA-mediated silencing of EWS-WT1 as in B. S9.6, RNA:DNA hybrids; ssDNA, loading control. **E.** Assessment of replication fork speed (kb/min) in RNaseH1-overexpressing JN1 cells subjected to siRNA-mediated silencing of EWS-WT1. Synchronized cells were collected 14 h post-transfection. A minimum of 50 forks were analyzed per condition. Mean ± SD, each dot represents a single replication fork; *n* = 2, unpaired t-test. **E.** Dose-response survival curves of JN1 cells exposed to PARPi talazoparib (F) or olaparib (G), and ATRi M4344 (H) or AZD6738 (I) for 7 days in presence or absence of siRNA-mediated silencing of EWS-WT1 and/or RNaseH1 overexpression. Mean ± SD; *n* = 3. Two-way ANOVA.

Figure 6. The combination of PARPi and ATRi elicits a cGAS/STING-mediated cell-autonomous immune response. A. Western blot of pTBK1, TBK, pIRF3, and IRF3 in JN1 cells exposed to DMSO control, PARPi talazoparib, ATRi M4344 or a combination of both for 72 h. **B, C**. RT-qPCR analysis of RNA isolated from JN1 cells exposed to DMSO control, PARPi talazoparib, ATRi M4344 or a combination of both for 72 h. CCL5 (B) and CXCL10 (C) mRNA were analyzed separately relative to RPLP0. Box-and-whisker plots show arbitrary units of gene expression, normalized to the DMSO condition. Boxes indicate median, lower and upper quartiles; whiskers indicate the 5th to 95th percentile range; n = 4, two-way ANOVA and post hoc Dunnett's test, relative to the DMSO condition. **D.** Quantification of PD-L1 cell-surface expression by flow cytometry in JN1 cells exposed to DMSO control, PARPi talazoparib, ATRi M4344 or a combination of both for 72 h. Scatter plot shows

the percentage of PD-L1-positive cells within the DAPI-negative population, normalized to the DMSO condition. Mean ± SD; n=3. Kruskal-Wallis test and post hoc Dunnett's test, relative to the DMSO condition. **E.** Western blot of pTBK1, TBK, pIRF3, and IRF3 in JN1 cells exposed to DMSO control, PARPi talazoparib, ATRi M4344 or a combination of both for 72 h, in presence or absence of siRNA-mediated silencing of EWS-WT1. **F, G.** RT-qPCR analysis of RNA isolated from JN1 cells exposed to DMSO control, PARPi talazoparib, ATRi M4344 or a combination of both for 72 h, in presence or absence of siRNA-mediated silencing of EWS-WT1. CCL5 (F) and CXCL10 (G) mRNA were analyzed separately relative to RPLP0. Box-and-whisker plots show arbitrary units of gene expression, normalized to the siCNTRL DMSO condition. Boxes indicate median and lower and upper quartiles; whiskers indicate the 5th to 95th percentile range; n = 4, two-way ANOVA and post hoc Dunnett's test, relative to the siCNTRL DMSO condition. **H.** Quantification of PD-L1 cell-surface expression by flow cytometry in JN1 cells exposed to DMSO control, PARPi talazoparib, ATRi M4344 or a combination of both for 72 h, in presence or absence of siRNA-mediated silencing of EWS-WT1. Scatter plot shows the percentage of PD-L1-positive cells within the DAPI-negative population, normalized to the siCNTRL DMSO condition. Mean ± SD; n=3. Kruskal-Wallis test and post hoc Dunnett's test, relative to the siCNTRL DMSO condition. **I.** Model of EWS-WT1-driven DSRCT sensitivity to PARPi and ATRi.

Figure 1.

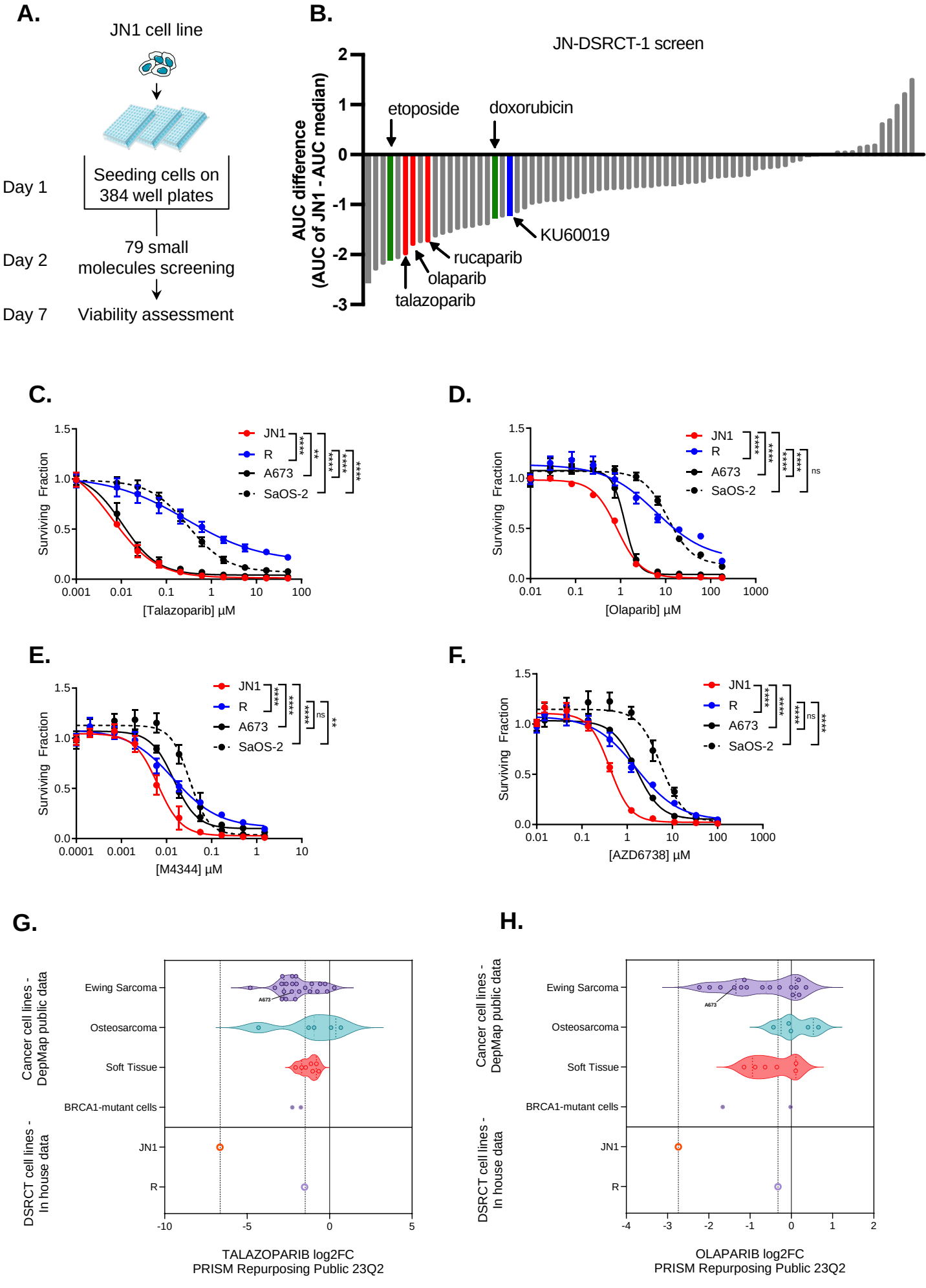
A.
JN1 cell line
Seeding cells on 384 well plates
Day 1
79 small molecules screening
Day 2
Viability assessment
Day 7
B.
JN-DSRCT-1 screen
AUC difference (AUC of JN1 - AUC median)
etoposide
doxorubicin
KU60019
rucaparib
olaparib
talazoparib
C.
Surviving Fraction
[Talazoparib] µM
JN1
R
A673
SaOS-2
D.
[Olaparib] µM
E.
[M4344] µM
F.
[AZD6738] µM
G.
Cancer cell lines - DepMap public data
DSRCT cell lines - In house data
Ewing Sarcoma
Osteosarcoma
Soft Tissue
BRCA1-mutant cells
TALAZOPARIB log2FC
PRISM Repurposing Public 23Q2
H.
OLAPARIB log2FC
PRISM Repurposing Public 23Q2

Figure 2.

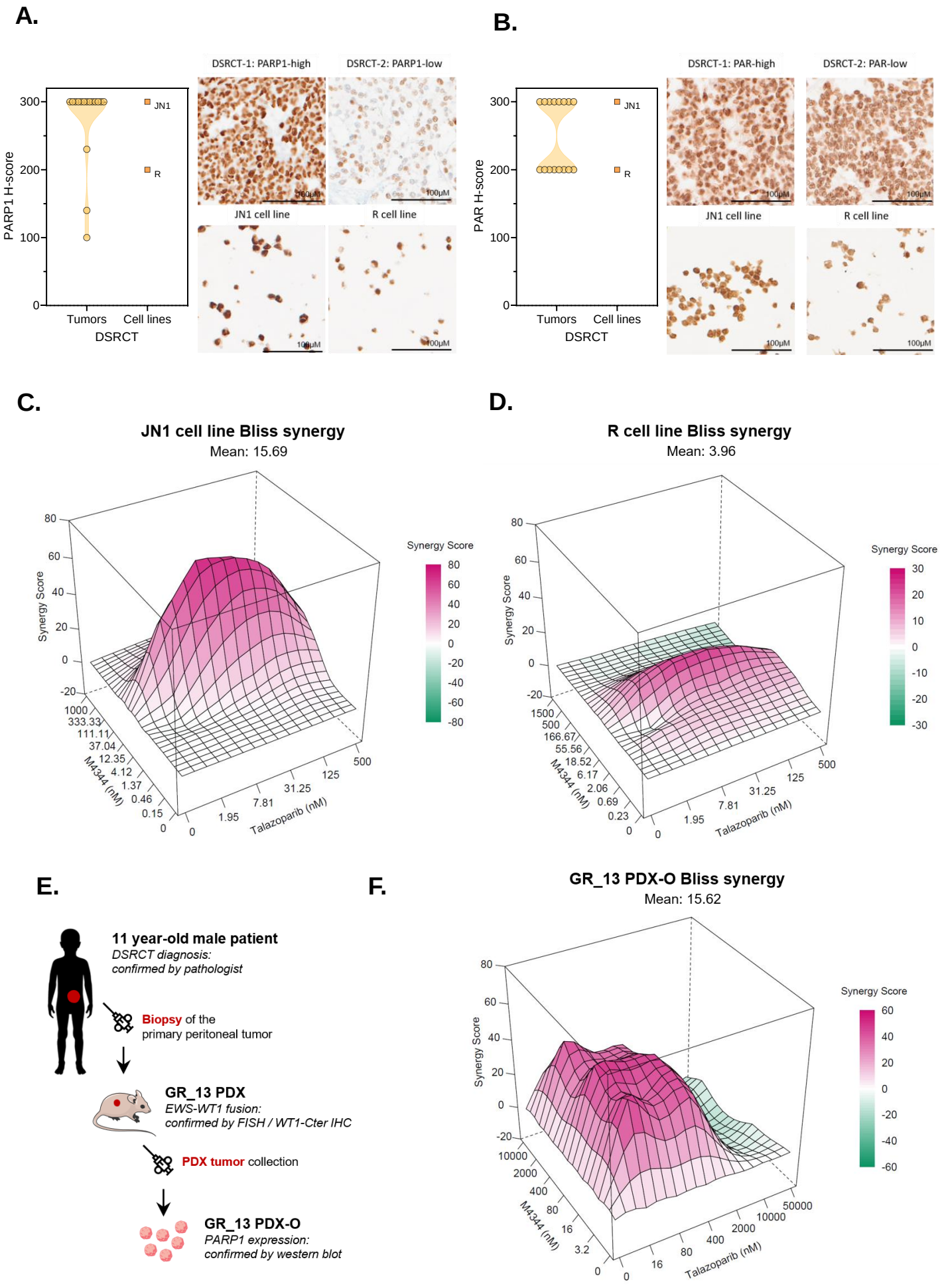
A.
PARP1 H-score
300
200
100
0
JN1
R
Tumors
Cell lines
DSRCT
DSRCT-1: PARP1-high
DSRCT-2: PARP1-low
JN1 cell line
R cell line
100µM
B.
PAR H-score
DSRCT-1: PAR-high
DSRCT-2: PAR-low
C.
JN1 cell line Bliss synergy
Mean: 15.69
Synergy Score
M4344 (nM)
Talazoparib (nM)
D.
R cell line Bliss synergy
Mean: 3.96
E.
11 year-old male patient
DSRCT diagnosis:
confirmed by pathologist
Biopsy of the
primary peritoneal tumor
GR_13 PDX
EWS-WT1 fusion:
confirmed by FISH / WT1-Cter IHC
PDX tumor collection
GR_13 PDX-O
PARP1 expression:
confirmed by western blot
F.
GR_13 PDX-O Bliss synergy
Mean: 15.62

Figure 3.

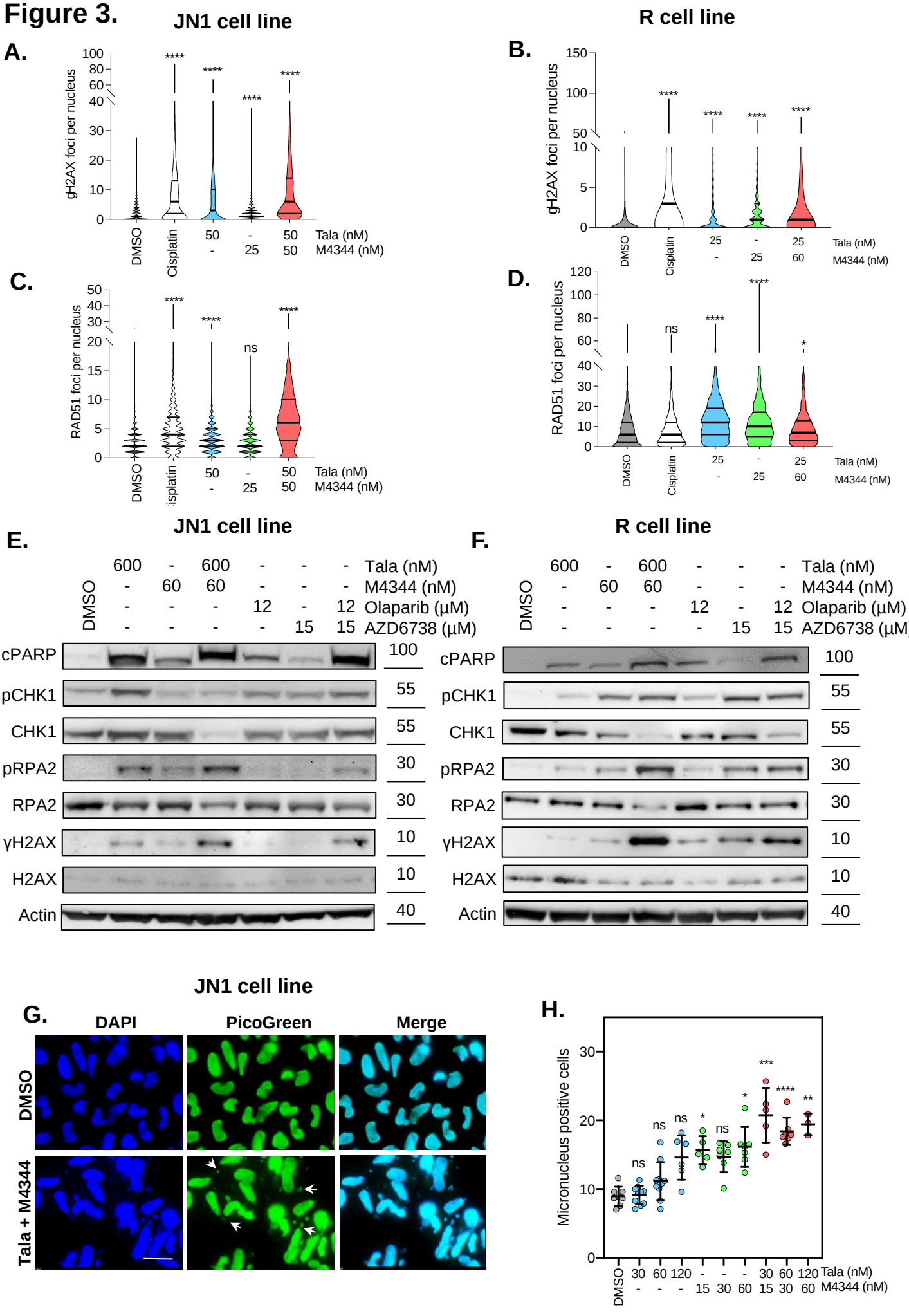
JN1 cell line
R cell line
A.
B.
C.
D.
γH2AX foci per nucleus
RAD51 foci per nucleus
DMSO
Cisplatin
Tala (nM)
M4344 (nM)
E.
F.
JN1 cell line
R cell line
Olaparib (μM)
AZD6738 (μM)
cPARP
pCHK1
CHK1
pRPA2
RPA2
γH2AX
H2AX
Actin
G.
JN1 cell line
DAPI
PicoGreen
Merge
DMSO
Tala + M4344
H.
Micronucleus positive cells

Figure 4.

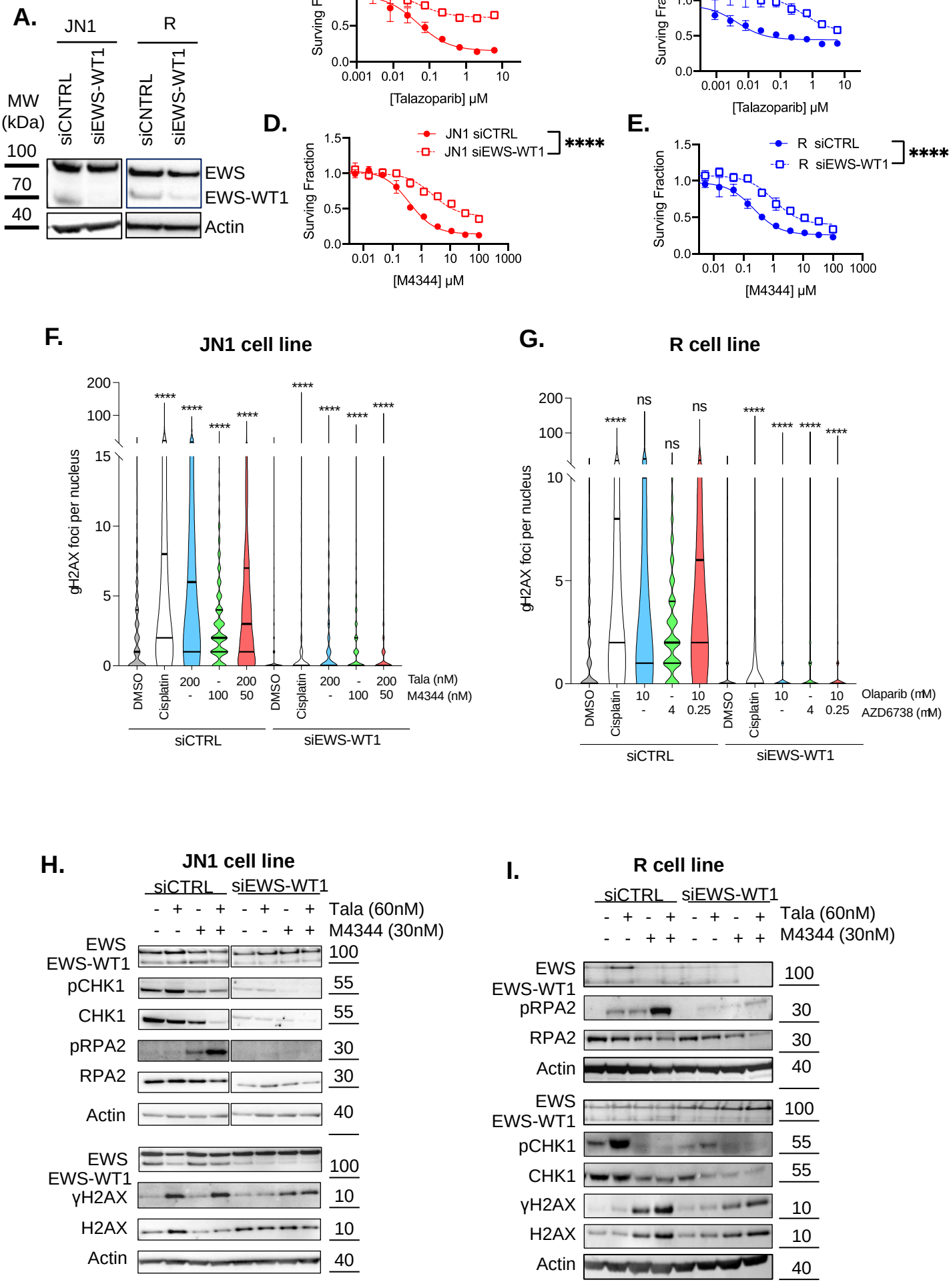
A.
JN1
R
siCNTRL
siEWS-WT1
siCNTRL
siEWS-WT1
MW (kDa)
100
70
40
EWS
EWS-WT1
Actin
B.
JN1 siCTRL
JN1 siEWS-WT1
****
Surving Fraction
[Talazoparib] µM
C.
R siCTRL
R siEWS-WT1
****
Surving Fraction
[Talazoparib] µM
D.
JN1 siCTRL
JN1 siEWS-WT1
****
Surving Fraction
[M4344] µM
E.
R siCTRL
R siEWS-WT1
****
Surving Fraction
[M4344] µM
F.
JN1 cell line
gH2AX foci per nucleus
DMSO
Cisplatin
200
-
100
200
50
Tala (nM)
M4344 (nM)
siCTRL
siEWS-WT1
G.
R cell line
gH2AX foci per nucleus
ns
DMSO
Cisplatin
10
-
4
10
0.25
Olaparib (nM)
AZD6738 (nM)
siCTRL
siEWS-WT1
H.
JN1 cell line
siCTRL
siEWS-WT1
Tala (60nM)
M4344 (30nM)
EWS
EWS-WT1
pCHK1
CHK1
pRPA2
RPA2
Actin
γH2AX
H2AX
I.
R cell line
siCTRL
siEWS-WT1
Tala (60nM)
M4344 (30nM)
EWS
EWS-WT1
pRPA2
RPA2
Actin
pCHK1
CHK1
γH2AX
H2AX
Actin

Figure 5.

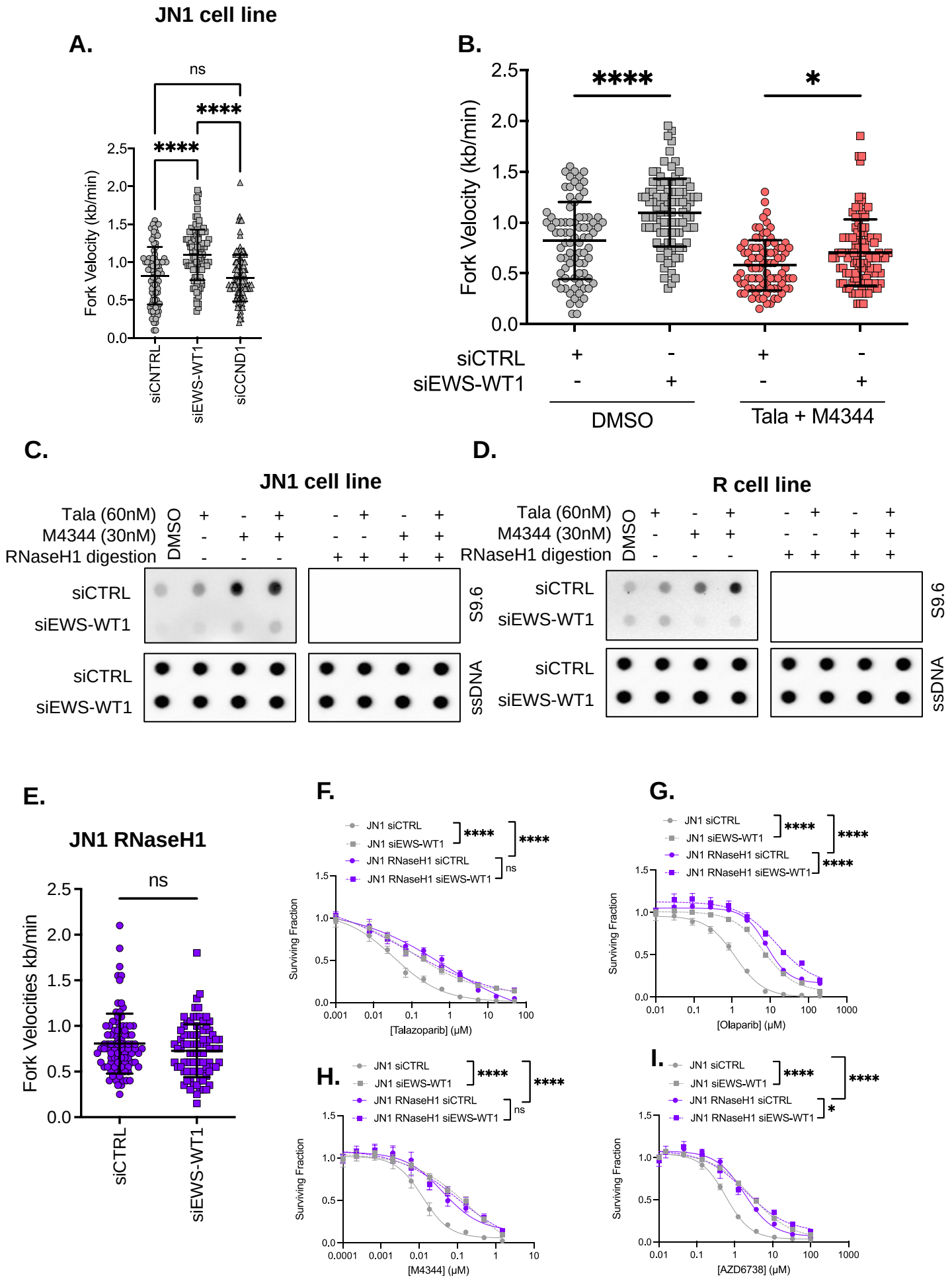
JN1 cell line
A.
ns
****
****
Fork Velocity (kb/min)
siCNTRL
siEWS-WT1
siCCND1
B.
****
*
Fork Velocity (kb/min)
siCTRL
siEWS-WT1
DMSO
Tala + M4344
C.
JN1 cell line
Tala (60nM)
M4344 (30nM)
RNaseH1 digestion
DMSO
siCTRL
siEWS-WT1
S9.6
ssDNA
D.
R cell line
Tala (60nM)
M4344 (30nM)
RNaseH1 digestion
DMSO
siCTRL
siEWS-WT1
S9.6
ssDNA
E.
JN1 RNaseH1
ns
Fork Velocities kb/min
siCTRL
siEWS-WT1
F.
JN1 siCTRL
JN1 siEWS-WT1
JN1 RNaseH1 siCTRL
JN1 RNaseH1 siEWS-WT1
****
****
ns
Surviving Fraction
[Talazoparib] (μM)
G.
JN1 siCTRL
JN1 siEWS-WT1
JN1 RNaseH1 siCTRL
JN1 RNaseH1 siEWS-WT1
****
****
****
Surviving Fraction
[Olaparib] (μM)
H.
JN1 siCTRL
JN1 siEWS-WT1
JN1 RNaseH1 siCTRL
JN1 RNaseH1 siEWS-WT1
****
****
ns
Surviving Fraction
[M4344] (μM)
I.
JN1 siCTRL
JN1 siEWS-WT1
JN1 RNaseH1 siCTRL
JN1 RNaseH1 siEWS-WT1
****
****
*
Surviving Fraction
[AZD6738] (μM)

Figure 6.

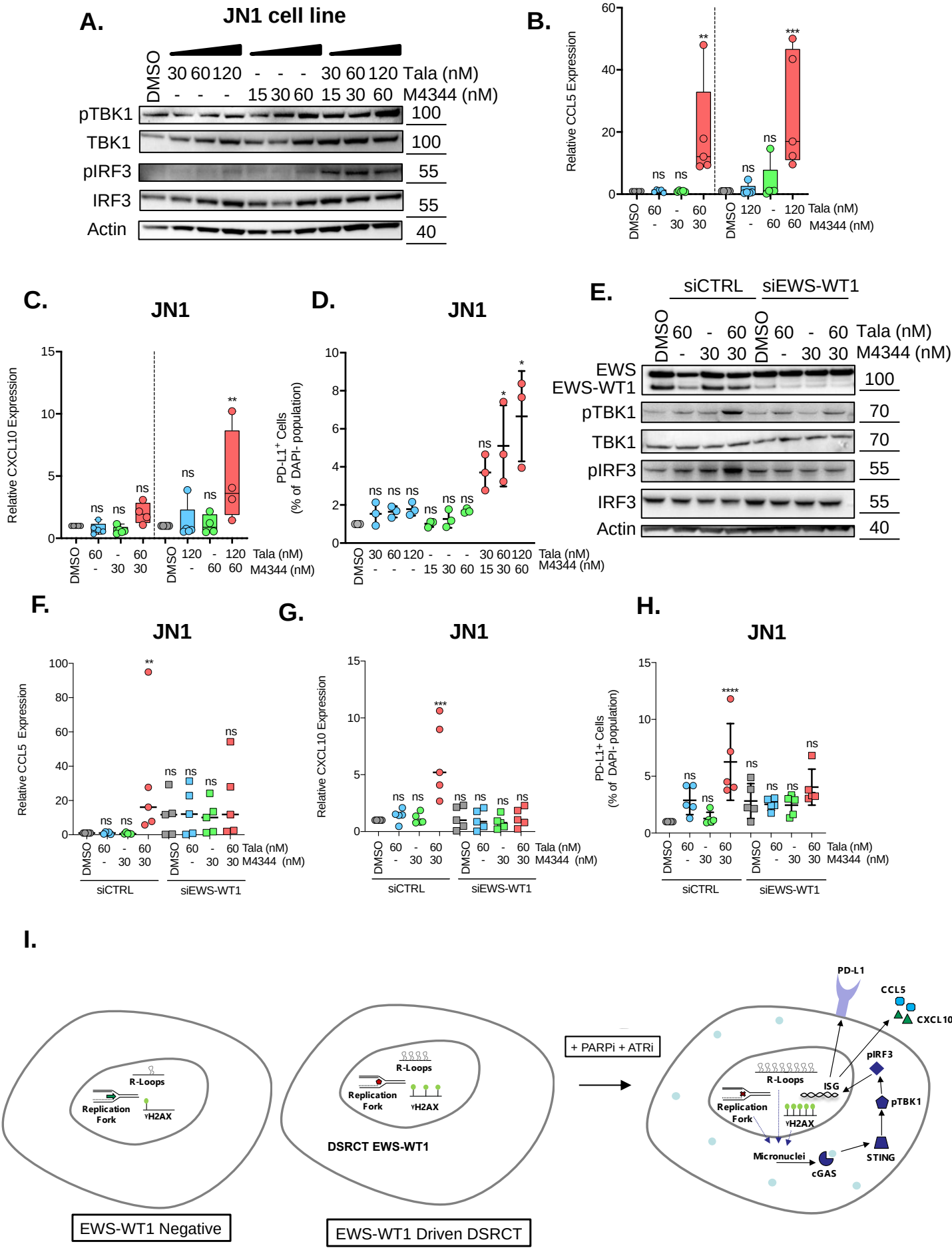
A.
JN1 cell line
DMSO
30 60 120 - - - 30 60 120 Tala (nM)
- - - 15 30 60 15 30 60 M4344 (nM)
pTBK1
TBK1
pIRF3
IRF3
Actin
100
100
55
55
40
B.
Relative CCL5 Expression
ns
**
***
DMSO 60 - 60 DMSO 120 - 120 Tala (nM)
- 30 30 - 60 60 M4344 (nM)
C.
JN1
Relative CXCL10 Expression
PD-L1+ Cells (% of DAPI- population)
D.
JN1
E.
siCTRL
siEWS-WT1
EWS
EWS-WT1
pTBK1
TBK1
pIRF3
IRF3
Actin
100
70
70
55
55
40
F.
JN1
Relative CCL5 Expression
siCTRL
siEWS-WT1
G.
JN1
Relative CXCL10 Expression
H.
JN1
PD-L1+ Cells (% of DAPI- population)
I.
R-Loops
Replication Fork
γH2AX
DSRCT EWS-WT1
+ PARPi + ATRi
PD-L1
CCL5
CXCL10
pIRF3
ISG
pTBK1
Micronuclei
cGAS
STING
EWS-WT1 Negative
EWS-WT1 Driven DSRCT

Parsed Citations

1. Subbiah V, Lamhamedi-Cherradi S-E, Cuglievan B, Menegaz BA, Camacho P, Huh W, et al. Multimodality Treatment of Desmoplastic Small Round Cell Tumor: Chemotherapy and Complete Cytoreductive Surgery Improve Patient Survival. Clin Cancer Res Off J Am Assoc Cancer Res. 2018;24:4865–73.
Pubmed: Author and Title
Google Scholar: Google Scholar Search

2. Cidre-Aranaz F, Watson S, Amatruda JF, Nakamura T, Delattre O, de Alava E, et al. Small round cell sarcomas. Nat Rev Dis Primer. 2022;8:66.
Pubmed: Author and Title
Google Scholar: Google Scholar Search

3. Mello CA, Campos FAB, Santos TG, Silva MLG, Torrezan GT, Costa FD, et al. Desmoplastic Small Round Cell Tumor: A Review of Main Molecular Abnormalities and Emerging Therapy. Cancers. 2021;13:498.
Pubmed: Author and Title
Google Scholar: Google Scholar Search

4. Chow WA, Yee J-K, Tsark W, Wu X, Qin H, Guan M, et al. Recurrent secondary genomic alterations in desmoplastic small round cell tumors. BMC Med Genet. 2020;21:101.
Pubmed: Author and Title
Google Scholar: Google Scholar Search

5. Slotkin EK, Bowman AS, Levine MF, Dela Cruz F, Coutinho DF, Sanchez GI, et al. Comprehensive Molecular Profiling of Desmoplastic Small Round Cell Tumor. Mol Cancer Res MCR. 2021;19:1146–55.
Pubmed: Author and Title
Google Scholar: Google Scholar Search

6. Wu C-C, Beird HC, Lamhamedi-Cherradi S-E, Soeung M, Ingram D, Truong DD, et al. Multi-site desmoplastic small round cell tumors are genetically related and immune-cold. NPJ Precis Oncol. 2022;6:21.
Pubmed: Author and Title
Google Scholar: Google Scholar Search

7. Devecchi A, De Cecco L, Dugo M, Penso D, Dagrada G, Brich S, et al. The genomics of desmoplastic small round cell tumor reveals the deregulation of genes related to DNA damage response, epithelial-mesenchymal transition, and immune response. Cancer Commun Lond Engl. 2018;38:70.
Pubmed: Author and Title
Google Scholar: Google Scholar Search

8. Vanoli F, Tomishima M, Feng W, Lamribet K, Babin L, Brunet E, et al. CRISPR-Cas9-guided oncogenic chromosomal translocations with conditional fusion protein expression in human mesenchymal cells. Proc Natl Acad Sci U S A. 2017;114:3696–701.
Pubmed: Author and Title
Google Scholar: Google Scholar Search

9. Gedminas JM, Chasse MH, McBrairty M, Beddows I, Kitchen-Goosen SM, Grohar PJ. Desmoplastic small round cell tumor is dependent on the EWS-WT1 transcription factor. Oncogenesis. 2020;9:41.
Pubmed: Author and Title
Google Scholar: Google Scholar Search

10. Bushweller JH. Targeting transcription factors in cancer - from undruggable to reality. Nat Rev Cancer. 2019;19:611–24.
Pubmed: Author and Title
Google Scholar: Google Scholar Search

11. Nishio J, Iwasaki H, Ishiguro M, Ohjimi Y, Fujita C, Yanai F, et al. Establishment and characterization of a novel human desmoplastic small round cell tumor cell line, JN-DSRCT-1. Lab Investig J Tech Methods Pathol. 2002;82:1175–82.

Pubmed: Author and Title
Google Scholar: Google Scholar Search

12. Holme H, Gulati A, Brough R, Fleuren EDG, Bajrami I, Campbell J, et al. Chemosensitivity profiling of osteosarcoma tumour cell lines identifies a model of BRCAness. Sci Rep. 2018;8:10614.
Pubmed: Author and Title
Google Scholar: Google Scholar Search

13. Bigot L, Sabio J, Poiraudeau L, Annereau M, Menssouri N, Helissey C, et al. Development of Novel Models of Aggressive Variants of Castration-resistant Prostate Cancer. Eur Urol Oncol. 2023;S2588-9311(23)00226-2.
Pubmed: Author and Title
Google Scholar: Google Scholar Search

14. Bialic M, Coulon V, Drac M, Gostan T, Schwob E. Analyzing the dynamics of DNA replication in mammalian cells using DNA combing. Methods Mol Biol. 2015;1300:67–78.
Pubmed: Author and Title
Google Scholar: Google Scholar Search

15. Gatz SA, Simón ARS, Archambaud B, Abbou S, Cleirec M, Leruste A, et al. Abstract CT019: Phase I/II study of the PARP inhibitor olaparib and ATR inhibitor ceralasertib in children with advanced malignancies: Arm N of the AcSé-ESMART trial. Cancer Res. 2023;83:CT019.
Pubmed: Author and Title
Google Scholar: Google Scholar Search

16. Goldstein MJ, Peters M, Weber BL, Davis CB. Optimizing the Therapeutic Window of Targeted Drugs in Oncology: Potency-Guided First-in-Human Studies. Clin Transl Sci. 2021;14:536–43.
Pubmed: Author and Title
Google Scholar: Google Scholar Search

17. Yap TA, Krebs MG, Postel-Vinay S, El-Khouiery A, Soria J-C, Lopez J, et al. Ceralasertib (AZD6738), an Oral ATR Kinase Inhibitor, in Combination with Carboplatin in Patients with Advanced Solid Tumors: A Phase I Study. Clin Cancer Res. 2021;
Pubmed: Author and Title
Google Scholar: Google Scholar Search

18. Burris HA, Berlin J, Arkenau T, Cote GM, Lolkema MP, Ferrer-Playan J, et al. A phase I study of ATR inhibitor gartisertib (M4344) as a single agent and in combination with carboplatin in patients with advanced solid tumours. Br J Cancer. 2024;130:1131–40.
Pubmed: Author and Title
Google Scholar: Google Scholar Search

19. Tlemsani C, Heske CM, Elloumi F, Pongor L, Khandagale P, Varma S, et al. Sarcoma_CellminerCDB: A tool to interrogate the genomic and functional characteristics of a comprehensive collection of sarcoma cell lines. iScience [Internet]. Elsevier; 2024 [cited 2024 Jun 28];27. Available from: https://www.cell.com/iscience/abstract/S2589-0042(24)01003-4

20. van Erp AEM, van Houdt L, Hillebrandt-Roeffen MHS, van Bree NFHN, Flucke UE, Mentzel T, et al. Olaparib and temozolomide in desmoplastic small round cell tumors: a promising combination in vitro and in vivo. J Cancer Res Clin Oncol. 2020;146:1659–70.
Pubmed: Author and Title
Google Scholar: Google Scholar Search

21. Pettitt SJ, Krastev DB, Brandsma I, Dréan A, Song F, Aleksandrov R, et al. Genome-wide and high-density CRISPR-Cas9 screens identify point mutations in PARP1 causing PARP inhibitor resistance. Nat Commun. 2018;9:1849.
Pubmed: Author and Title
Google Scholar: Google Scholar Search

22. Murai J, Huang SN, Das BB, Renaud A, Zhang Y, Doroshow JH, et al. Trapping of PARP1 and PARP2 by Clinical PARP Inhibitors. Cancer Res. 2012;72:5588–99.

Pubmed: Author and Title
Google Scholar: Google Scholar Search

23. Pommier Y, O'Connor MJ, de Bono J. Laying a trap to kill cancer cells: PARP inhibitors and their mechanisms of action. Sci Transl Med. 2016;8:362ps17.
Pubmed: Author and Title
Google Scholar: Google Scholar Search

24. Henon C, Vibert J, Eychenne T, Gruel N, Colmet-Daage L, Ngo C, et al. Single-cell multiomics profiling reveals heterogeneous transcriptional programs and microenvironment in DSRCTs. Cell Rep Med. 2024;5:101582.
Pubmed: Author and Title
Google Scholar: Google Scholar Search

25. Bomgaars LR, Bernstein M, Krailo M, Kadota R, Das S, Chen Z, et al. Phase II trial of irinotecan in children with refractory solid tumors: a Children's Oncology Group Study. J Clin Oncol Off J Am Soc Clin Oncol. 2007;25:4622–7.
Pubmed: Author and Title
Google Scholar: Google Scholar Search

26. Banerji U, Plummer ER, Moreno V, Ang JE, Quinton A, Drew Y, et al. A phase I/II first-in-human trial of oral SRA737 (a Chk1 inhibitor) given in combination with low-dose gemcitabine in subjects with advanced cancer. J Clin Oncol. Wolters Kluwer; 2019;37:3095–3095.
Pubmed: Author and Title
Google Scholar: Google Scholar Search

27. Kiesel BF, Scemama J, Parise RA, Villaruz L, Iffland A, Doyle A, et al. LC-MS/MS assay for the quantitation of the ATR kinase inhibitor VX-970 in human plasma. J Pharm Biomed Anal. 2017;146:244–50.
Pubmed: Author and Title
Google Scholar: Google Scholar Search

28. Zanoni M, Piccinini F, Arienti C, Zamagni A, Santi S, Polico R, et al. 3D tumor spheroid models for in vitro therapeutic screening: a systematic approach to enhance the biological relevance of data obtained. Sci Rep. Nature Publishing Group; 2016;6:19103.
Pubmed: Author and Title
Google Scholar: Google Scholar Search

29. Bleijs M, van de Wetering M, Clevers H, Drost J. Xenograft and organoid model systems in cancer research. EMBO J. John Wiley & Sons, Ltd; 2019;38:e101654.
Pubmed: Author and Title
Google Scholar: Google Scholar Search

30. Magrath JW, Kang H-J, Hartono A, Espinosa-Cotton M, Somwar R, Ladanyi M, et al. Desmoplastic small round cell tumor cancer stem cell-like cells resist chemotherapy but remain dependent on the EWSR1-WT1 oncoprotein. Front Cell Dev Biol. 2022;10:1048709.
Pubmed: Author and Title
Google Scholar: Google Scholar Search

31. Horning JL, Sahoo SK, Vijayaraghavalu S, Dimitrijevic S, Vasir JK, Jain TK, et al. 3-D tumor model for in vitro evaluation of anticancer drugs. Mol Pharm. 2008;5:849–62.
Pubmed: Author and Title
Google Scholar: Google Scholar Search

32. Buisson R, Niraj J, Rodrigue A, Ho CK, Kreuzer J, Foo TK, et al. Coupling of Homologous Recombination and the Checkpoint by ATR. Mol Cell. 2017;65:336–46.
Pubmed: Author and Title
Google Scholar: Google Scholar Search

33. Lord CJ, Ashworth A. PARP inhibitors: Synthetic lethality in the clinic. Science. 2017;355:1152–8.
Pubmed: Author and Title
Google Scholar: Google Scholar Search

34. Groelly FJ, Fawkes M, Dagg RA, Blackford AN, Tarsounas M. Targeting DNA damage response pathways in cancer. Nat Rev Cancer. 2023;23:78–94.
Pubmed: Author and Title
Google Scholar: Google Scholar Search

35. da Costa AABA, Chowdhury D, Shapiro GI, D'Andrea AD, Konstantinopoulos PA. Targeting replication stress in cancer therapy. Nat Rev Drug Discov. 2023;22:38–58.
Pubmed: Author and Title
Google Scholar: Google Scholar Search

36. Liu J, Nau MM, Yeh JC, Allegra CJ, Chu E, Wright JJ. Molecular heterogeneity and function of EWS-WT1 fusion transcripts in desmoplastic small round cell tumors. Clin Cancer Res Off J Am Assoc Cancer Res. 2000;6:3522–9.
Pubmed: Author and Title
Google Scholar: Google Scholar Search

37. Gorthi A, Romero JC, Loranc E, Cao L, Lawrence LA, Goodale E, et al. EWS-FLI1 increases transcription to cause R-Loops and block BRCA1 repair in Ewing sarcoma. Nature. 2018;555:387–91.
Pubmed: Author and Title
Google Scholar: Google Scholar Search

38. Petermann E, Lan L, Zou L. Sources, resolution and physiological relevance of R-loops and RNA-DNA hybrids. Nat Rev Mol Cell Biol. 2022;23:521–40.
Pubmed: Author and Title
Google Scholar: Google Scholar Search

39. Kotsantis P, Silva LM, Irmscher S, Jones RM, Folkes L, Gromak N, et al. Increased global transcription activity as a mechanism of replication stress in cancer. Nat Commun. 2016;7:13087.
Pubmed: Author and Title
Google Scholar: Google Scholar Search

40. Groelly FJ, Dagg RA, Petropoulos M, Rossetti GG, Prasad B, Panagopoulos A, et al. Mitotic DNA synthesis is caused by transcription-replication conflicts in BRCA2-deficient cells. Mol Cell. 2022;82:3382-3397.e7.
Pubmed: Author and Title
Google Scholar: Google Scholar Search

41. Chabanon RM, Morel D, Eychenne T, Colmet-Daage L, Bajrami I, Dorvault N, et al. PBRM1 Deficiency Confers Synthetic Lethality to DNA Repair Inhibitors in Cancer. Cancer Res. 2021;81:2888–902.
Pubmed: Author and Title
Google Scholar: Google Scholar Search

42. Bayona-Feliu A, Barroso S, Muñoz S, Aguilera A. The SWI/SNF chromatin remodeling complex helps resolve R-loop-mediated transcription-replication conflicts. Nat Genet. 2021;53:1050–63.
Pubmed: Author and Title
Google Scholar: Google Scholar Search

43. Motwani M, Pesiridis S, Fitzgerald KA. DNA sensing by the cGAS-STING pathway in health and disease. Nat Rev Genet. 2019;20:657–74.
Pubmed: Author and Title
Google Scholar: Google Scholar Search

44. Samson N, Ablasser A. The cGAS-STING pathway and cancer. Nat Cancer. 2022;3:1452–63.
Pubmed: Author and Title
Google Scholar: Google Scholar Search

45. Chabanon RM, Muirhead G, Krastev DB, Adam J, Morel D, Garrido M, et al. PARP inhibition enhances tumor cell–intrinsic immunity in ERCC1-deficient non–small cell lung cancer. J Clin Invest. 2019;129:1211–28.
Pubmed: Author and Title
Google Scholar: Google Scholar Search

46. Pantelidou C, Sonzogni O, Taveira MDO, Mehta AK, Kothari A, Wang D, et al. PARP inhibitor efficacy depends on CD8+ T-cell recruitment via intratumoral STING pathway activation in BRCA-deficient models of triple-negative breast cancer. Cancer Discov. 2019;9:722–37.
Pubmed: Author and Title
Google Scholar: Google Scholar Search

47. Ding L, Kim HJ, Wang Q, Kearns M, Jiang T, Ohlson CE, et al. PARP Inhibition Elicits STING-Dependent Antitumor Immunity in Brca1-Deficient Ovarian Cancer. Cell Rep. 2018;25:2972–80.
Pubmed: Author and Title
Google Scholar: Google Scholar Search

48. Reisländer T, Lombardi EP, Groelly FJ, Miar A, Porru M, Di Vito S, et al. BRCA2 abrogation triggers innate immune responses potentiated by treatment with PARP inhibitors. Nat Commun. 2019;10:3143–3143.
Pubmed: Author and Title
Google Scholar: Google Scholar Search

49. Wang Z, Sun K, Xiao Y, Feng B, Mikule K, Ma XY, et al. Niraparib activates interferon signaling and potentiates anti-PD-1 antibody efficacy in tumor models. Sci Rep. 2019;9:1853–1853.
Pubmed: Author and Title
Google Scholar: Google Scholar Search

50. Feng X, Tubbs A, Zhang C, Tang M, Sridharan S, Wang C, et al. ATR inhibition potentiates ionizing radiation-induced interferon response via cytosolic nucleic acid-sensing pathways. EMBO J. 2020;39:e104036–e104036.
Pubmed: Author and Title
Google Scholar: Google Scholar Search

51. Pettitt SJ, Rehman FL, Bajrami I, Brough R, Wallberg F, Kozarewa I, et al. A genetic screen using the PiggyBac transposon in haploid cells identifies Parp1 as a mediator of olaparib toxicity. PloS One. 2013;8:e61520.
Pubmed: Author and Title
Google Scholar: Google Scholar Search

52. Lowery CD, Dowless M, Renschler M, Blosser W, VanWye AB, Stephens JR, et al. Broad Spectrum Activity of the Checkpoint Kinase 1 Inhibitor Prexasertib as a Single Agent or Chemopotentiator Across a Range of Preclinical Pediatric Tumor Models. Clin Cancer Res Off J Am Assoc Cancer Res. 2019;25:2278–89.
Pubmed: Author and Title
Google Scholar: Google Scholar Search

53. Slotkin EK, Mauguen A, Ortiz MV, Dela Cruz FS, O'Donohue T, Kinnaman MD, et al. A phase I/II study of prexasertib in combination with irinotecan in patients with relapsed/refractory desmoplastic small round cell tumor and rhabdomyosarcoma. J Clin Oncol. Wolters Kluwer; 2022;40:11503–11503.
Pubmed: Author and Title
Google Scholar: Google Scholar Search

54. Mahdi H, Hafez N, Doroshow D, Sohal D, Keedy V, Do KT, et al. Ceralasertib-Mediated ATR Inhibition Combined With Olaparib in Advanced Cancers Harboring DNA Damage Response and Repair Alterations (Olaparib Combinations). JCO Precis Oncol. 2021;5:PO.20.00439.
Pubmed: Author and Title
Google Scholar: Google Scholar Search

55. Brenner JC, Feng FY, Han S, Patel S, Goyal SV, Bou-Maroun LM, et al. PARP-1 inhibition as a targeted strategy to treat Ewing's sarcoma. Cancer Res. 2012;72:1608–13.
Pubmed: Author and Title
Google Scholar: Google Scholar Search

56. Pearson ADJ, Zwaan CM, Kolb EA, Karres D, Guillot J, Kim SY, et al. Paediatric Strategy Forum for medicinal product development for acute myeloid leukaemia in children and adolescents: ACCELERATE

in collaboration with the European Medicines Agency with participation of the Food and Drug Administration. Eur J Cancer Oxf Engl 1990. 2020;136:116–29.
Pubmed: Author and Title
Google Scholar: Google Scholar Search

57. Tumini E, Herrera-Moyano E, San Martín-Alonso M, Barroso S, Galmarini CM, Aguilera A. The Antitumor Drugs Trabectedin and Lurbinectedin Induce Transcription-Dependent Replication Stress and Genome Instability. Mol Cancer Res MCR. 2019;17:773–82.
Pubmed: Author and Title
Google Scholar: Google Scholar Search

58. Grignani G, D'Ambrosio L, Pignochino Y, Palmerini E, Zucchetti M, Boccone P, et al. Trabectedin and olaparib in patients with advanced and non-resectable bone and soft-tissue sarcomas (TOMAS): an open-label, phase 1b study from the Italian Sarcoma Group. Lancet Oncol. 2018;19:1360–71.
Pubmed: Author and Title
Google Scholar: Google Scholar Search

59. Merlini A, Centomo ML, Ferrero G, Chiabotto G, Miglio U, Berrino E, et al. DNA damage response and repair genes in advanced bone and soft tissue sarcomas: An 8-gene signature as a candidate predictive biomarker of response to trabectedin and olaparib combination. Front Oncol. 2022;12:844250.
Pubmed: Author and Title
Google Scholar: Google Scholar Search

60. Chabanon RM, Rouanne M, Lord CJ, Soria J-C, Pasero P, Postel-Vinay S. Targeting the DNA damage response in immuno-oncology: developments and opportunities. Nat Rev Cancer. 2021;21:701–17.
Pubmed: Author and Title
Google Scholar: Google Scholar Search

61. Besse B, Awad MM, Forde PM, Thomas M, Goss G, Aronson B, et al. OA15.05 HUDSON: An Open-Label, Multi-Drug, Biomarker-Directed Phase 2 Study in NSCLC Patients Who Progressed on Anti-PD-(L)1 Therapy. J Thorac Oncol. 2022;17:S41–2.
Pubmed: Author and Title
Google Scholar: Google Scholar Search

62. Iyer S, Conway J, Russell D, Reddy A, Cosaert J, Barry S, et al. Abstract CT039: Immunomodulatory effects of ceralasertib in combination with durvalumab in patients with NSCLC and progression on anti-PD-(L)1 treatment (HUDSON, NCT03334617). Cancer Res. 2023;83:CT039.
Pubmed: Author and Title
Google Scholar: Google Scholar Search

63. Kim R, Kwon M, An M, Kim ST, Smith SA, Loembé AB, et al. Phase II study of ceralasertib (AZD6738) in combination with durvalumab in patients with advanced/metastatic melanoma who have failed prior anti-PD-1 therapy. Ann Oncol Off J Eur Soc Med Oncol. 2022;33:193–203.
Pubmed: Author and Title
Google Scholar: Google Scholar Search